6-17-2024

Fabrication of Metallo-Pharmaceutical Composite Hydrogel Composed of Curcumin-Loaded CMC-Na/Sodium Alginate/PdCl2: Optimization, Antimicrobial Activity, and Cancer Cell Mortality In Vitro Assessment

samar A. salim

Elbadawy A Kamoun

mariam emam

Shahira H El-Moslamy

ayman elsawaf

See next page for additional authors

Authors

samar A. salim, Elbadawy A Kamoun, mariam emam, Shahira H El-Moslamy, ayman elsawaf, amal nassar, and nehal eldeeb

Arabian Journal for Science and Engineering
https://doi.org/10.1007/s13369-024-09233-w

RESEARCH ARTICLE-CHEMISTRY

Fabrication of Metallo-Pharmaceutical Composite Hydrogel Composed of Curcumin-Loaded CMC-Na/Sodium Alginate/$PdCl_2$: Optimization, Antimicrobial Activity, and Cancer Cell Mortality In Vitro Assessment

Elbadawy A. Kamoun[1,2] · Mariam M. Imam[3] · Shahira H. EL-Moslamy[4] · Ayman K. El-Sawaf[5,6] · Amal A. Nassar[6] · Nehal M. El-Deeb[7] · Samar A. Salim[3]

Received: 9 November 2023 / Accepted: 26 May 2024

Abstract

This work explores the fabrication route of curcumin-loaded carboxymethyl cellulose sodium/sodium alginate/palladium chloride (CMC-Na/SA/$PdCl_2$) composite hydrogel as localized delivery system for cancer treatment. Herein, an approach was established for improving encapsulation capacity and exploiting therapeutic efficiency. CMC-Na/SA/$PdCl_2$ composite hydrogels were prepared by gelation method using ionic crosslinker ($PdCl_2$). Results proved that the optimized formula (CMC-Na:SA (4:1)/$PdCl_2$ 0.4%) recorded a gel fraction of 91% with a swelling ratio ~ 3000% after 96 h, while XRD analysis exhibited no remarks of sharp peaks which confirmed an amorphous phase of tested hydrogel. TGA results showed that this recipe is thermostable compared to other tested formulae. Moreover, SEM of crosslinked unloaded and curcumin-loaded hydrogel showed interconnected pores indicating the interior crosslinked chains formed. According to FT-IR analysis, curcumin was incorporated successfully into CMC-Na/SA via intermolecular hydrogen bonding between curcumin and hydrogel components. In vitro cytotoxicity of CMC-Na/SA/$PdCl_2$ hydrogel exhibited an inhibition proliferation for breast cancer cells (*MDA-MB231*), liver cancer cells (*HePG-2*), and colon cancer cells (*CaCo-2*) without any toxic effect on the normal cells. Additionally, curcumin-loaded CMC-Na/SA/$PdCl_2$ composite hydrogels exhibited only 50% inhibition proliferation for *HePG-2* with 0.6% curcumin. Also, curcumin-free crosslinked CMC-Na/SA (4:1) hydrogels exhibited 80% inhibition proliferation for *HePG-2* cells. According to antimicrobial bioassay data, CMC-Na:SA (4:1)/$PdCl_2$ 0.4%/0.6% Cr hydrogel has the maximum biofilm inhibition as was recorded against *Staphylococcus aureus* (77%), followed by *Bacillus cereus* (74%) and *Candida krusei* (66%). Thus, CMC-Na/SA/$PdCl_2$ composite hydrogels could be regarded as promising antibacterial and anticancer biomaterials for multipurpose biomedical applications.

Keywords CMC/SA composite hydrogel · $PdCl_2$ · Curcumin · Antibacterial activity

✉ Elbadawy A. Kamoun
ekamoun@kfu.edu.sa; badawykamoun@yahoo.com

✉ Samar A. Salim
Samar.salim@bue.edu.eg

[1] Department of Chemistry, College of Science, King Faisal University, 31982 Al-Ahsa, Saudi Arabia

[2] Polymeric Materials Research Department, Advanced Technology and New Materials Research Institute (ATNMRI), City of Scientific Research and Technological Applications (SRTA-City), New Borg El-Arab City, Alexandria 21934, Egypt

[3] Biomaterials for Medical and Pharmaceutical Applications Research Group, Nanotechnology Research Center (NTRC), The British University in Egypt (BUE), Cairo 11837, Egypt

[4] Bioprocess Development Department (BID), Genetic Engineering and Biotechnology Research Institute (GEBRI), City of Scientific Research and Technological Applications (SRTA-City), New Borg El-Arab City, Alexandria 21934, Egypt

[5] Department of Chemistry, Collage of Science and Humanities in Al-Kharj, Prince Sattam Bin Abdulaziz University, 11942 Al-Kharj, Saudi Arabia

[6] Department of Chemistry, Faculty of Science, Menoufia University, Shebin El-Kom, Egypt

[7] Pharmaceutical and Fermentation Industries Development Center, City of Scientific Research and Technological Applications (SRTA-City, New Borg El-Arab City, Alexandria, Egypt

Published online: 17 June 2024

1 Introduction

Hydrogel is one of biomaterials that is broadly utilized in different disciplines of biomedical applications due to their high biocompatibility, controllable swelling manner, flexibility, and their simple procedure conditions. Their unique properties broaden their application potential in bone and cartilage regeneration, targeted drug delivery, tissue engineering, electrical and soft robotic components, biosensors and wound healing [1]. The main downside of hydrophilic polysaccharide polymers is that they degrade more quickly with lowering stability in water, while this obstacle could be improved by adding crosslinker to the system [2]. To increase the crosslinking density and provide hydrogels with greater functional qualities, researchers began utilizing chemical and metal ions as crosslinkers. Covalent bonds produced by chemical crosslinking give rise to irreversible connections; in contrast, dynamic crosslinking produced by metal ion crosslinking is reversible in nature. Even few amounts of chemical crosslinkers often lead to cell toxicity and unfavorable interaction of other biological components [3]. In physical crosslinked hydrogels, secondary interactions such as ionic crosslinks, H–H bonds, and hydrophobic interactions hold the polymeric chains together. On the other hand, chemical gels have irreversible covalent bonds that hold the polymeric chains together [4].

Utilizing inorganic metal ions provides crosslinking, stability, and various benefits for the biological processes in the body which are primarily compatible with the structure of proteins (Zn and Ca), nucleic acids (Mn and Mg), charge balance (Na, K, and Ca), redox catalysis (Fe, Co, Ni, V, Mn, Cu, and W), acid–base catalysis (Fe, Zn, Mg, Ni, and Mn), bone structure (Ca, Si), and DNA signaling (Co, Ag, Pb, As, Sb, Cd, Ni, Hg, Cu, Zn, Fe, and Mn) [3]. Furthermore, replacing harmful chemical crosslinkers with safe ones leads to avoiding the risk of cytotoxicity from unreacted chemical crosslinkers and producing stimuli-responsive, self-healing, and injectable at room temperature hydrogels [5].

One of the most flexible transition metals palladium is widely used in academia, health, and industry. Palladium (Pd) is used as catalyst in the synthesis of a variety of organic molecules, including medicines, heteroarenes, natural products, also as a catalyst in C–C coupling, C–H functionalization, and hydrocarbon oxidation processes [6]. It is commonly employed as a pollution management tool for eliminating organic pollutants [7]. Hanafy et al. have reported an excellent catalytic system for the oxidation of polyphenolic compounds using a variety of Pd-containing poly(vinyl alcohol) hydrogel samples with varying amounts of palladium chloride, who proved that PVA can bond with transition metal ions due to abundance of –OH groups on its surface [6].

Recently, palladium complexes have considerable anticancer activity, as well as lower toxicity compared with some commonly used chemotherapeutics [8]. Palladium nanoparticles (Pd NPs) have been found its potential therapeutic characteristics for the biomedical applications [9–11]. It has been reported that designed Pd complexes of types (NHC) Pd (pyridine) Cl_2 and $(NHC)_2PdCl_2$ display powerful anticancer activity. It was found that $(NHC)_2PdCl_2$ inhibited the proliferation of *HeLa, MCF-7*, and *HCT 116* cells in culture at low micromolar doses, which are noticeably sturdier than the inhibitory of the most used drug and cisplatin [12].

Sodium alginate (SA) as a natural product has been intensively researched for a wide range of biological applications, due to its low cost, biocompatibility, biodegradability, and simplicity of chemical derivatization. SA hydrogels have been particularly appealing in wound healing and tissue engineering purposes, owing to their structural likenesses to extracellular matrices in tissues [13]. SA has been shown to be a linear hydrophilic polysaccharide composed of 1,4-linked β-*D*-mannuronic (M block) and α-*L*-guluronic acid (G block) [14].

Moreover, carboxymethyl cellulose (CMC) is a thickener synthetic cellulose, viscosity modifier, and water retainer agent, which is non-toxic, biocompatible, and biodegradable. Physical and chemical properties of CMC can be enhanced via copolymerization with various polymers which makes little modifications to its nature. Many studies have shown that CMC-based hydrogels have the potential for a variety of biomedical applications, counting drug carriers [15], wound dressing [16], injectable hydrogels [17], and tissue engineering scaffolds [18]. The abundance of hydroxyl ($–OH^-$) and carboxylate ($–COO^-$) groups in CMC gives it an advantage in biomaterials development [19]. Koneru et al. have prepared sodium carboxymethylcellulose–grapefruit seed extract nanocomposite hydrogel films and demonstrated that these films have a proven ability to serve as wound healing materials since they show an excellent antimicrobial property [20].

SA/CMC-Na-based hydrogel beads were previously prepared by calcium chloride as ionic crosslinker for sustained drug delivery, antibacterial activity, and Pb(II) adsorption applications respectively [21, 22]. Also, Zhang et al. used calcium chloride as ionic crosslinker and demonstrated that SA/CMC-Na (4:1) combined hydrogel may produce a healing performance comparable to autologous skin implanting. It was concluded that under the same deformation condition, SA/Na-CMC (4:1) had the best compression performance, followed by SA/CMC-Na (8:1), and both were more effective than pure SA [23].

Plant-derived natural components have become a core area of interest, due to the growth of drug resistance and efforts to

improve cancer therapy, especially since the malignant condition endangers the lives of many people worldwide. Curcumin (Cr), also known as diferuloyl methane, is the primary curcuminoid present in *curcuma longa*. It is a linear diarylheptanoid (E,E)-1,7-bis(4-hydroxy-3-methoxyphenyl)-1,6-heptadiene3,5-dione [24]. Numerous studies have demonstrated its potential as a potent antioxidant, chemo-preventive agent for various malignancies, anti-atherosclerotic, antiviral [25], antifungal [26], and antibacterial [27], hepatoprotective agent [28], general wound healing enhancer [29], and a variety of other advantageous effects. Curcumin has powerful antioxidant activity at low concentrations. It paradoxically acts as a pro-oxidant substance at higher quantities, which is advantageous for the treatment of cancer [30]. Hussein et al. prepared PVA/CNCs/curcumin membrane, and these composite membranes showed sustained-release profile and remarkable anticancer features demonstrated by its cytotoxic impact on both *Huh-7* and *MCF-7* cell lines without upsetting viability fraction of *HFB-4* cells, in addition to notable antimicrobial action beside tested pathogenic microbes [31].

Herein, we are exploring a simple preparation route for formation of curcumin-loaded $PdCl_2$ crosslinked CMC-Na/SA composite hydrogels. The results demonstrated the physicochemical features of all prepared composite hydrogels, where their biocompatibility, antimicrobial effect, anticancer effect, and potential as an alternative and well-designed biomaterial for cancer treatment were assessed and discussed in detail.

2 Materials and Methods

2.1 Materials

Sodium alginate (SA, general purpose grade, medium viscosity) and sodium salt of CMC (granules, Mwt. ~ 250,000 g/mol, DS = 0.7) were purchased from Acros Organic, Belgium. Palladium (II) chloride ($PdCl_2$, analytically pure $\geq$ 99.9%) was from Sigma-Aldrich, Germany. Curcumin (95%, total *curcuminoid* content) was obtained from Alfa Aesar, Germany. *WI-38* cell line (CCL-25) (normal epithelial cells, human), *MDA-MB-231* cell line (HTB-26) (mammary gland/breast adenocarcinoma, human), *CaCo-2* cell line (CaCo-2, HTB-37) (colorectal adenocarcinoma, epithelial cells, human), and *HepG-2 (HEPG2, HB-8065)* (human, liver hepatocellular carcinoma) were obtained from The Global Bioresource Center (ATCC), USA, with aforementioned product catalog of human and animal cell lines for research purposes. DMEM media was employed to culture the subsequent cell lines, *CaCo-2*, and *WI-38*, while *MDA-MB-231* and *HepG-2* cell lines were grown on RBMI media. All culture media were supplemented with 10.0% fetal bovine serum (Lonza), 200 mM L-glutamine, and 1.0% penicillin/streptomycin antibiotic solution (Lonza). Cells were seeded into tissue culture flasks (25.0 cm) and incubated at 37 °C under 5.0% CO_2 for 24 h or till confluency. In this work, the tested human pathogens (*Salmonella paratyphi, Escherichia coli, Pseudomonas aeruginosa, Staphylococcus epidermidis, Staphylococcus aureus, Bacillus cereus, Candida krusei, Candida tropical,* and *Candida glabrata*) were received from Bioprocess Development Dep., GEBRI, SRTA-City, Egypt.

2.2 Preparation of Curcumin-Loaded and Unloaded CMC-Na/SA/$PdCl_2$ Composite Hydrogel

First, the stocks of 2% (wt./v) SA and 2% (wt./v) of CMC-Na were prepared using deionized water at 50 ºC, where the stocks were stored at fridge at 4ºC for a maximum three days. The different composition ratios of SA:CMC-Na were set at 1:1, 2:1, 4:1, 1:4, and 1:2, correspondingly. The mixture solution was agitated at 65ºC for two hours until obtaining homogeneous mixtures. After SA/CMC-Na solutions were fully mixed, they were removed and achieved degassing by degasser. Different concentrations of $PdCl_2$ dispersed solutions were prepared as follows: 0.1, 0.2, 0.4, and 0.6% (wt./v). The different quantities of $PdCl_2$ were weighted based on the specific concentration and then well dispersed into 5 ml deionized water using water bath sonication for a time, not less than three hours.

Crosslinked CMC-Na/SA can be obtained immediately after injection of $PdCl_2$ solution as droplets using a plastic syringe into different sites of the bottom of CMC-Na/SA solution with continuous stirring at 37 °C until complete miscibility and ideal hydrogel formation. This method is similar to little adjustments to that used by Agarwal et al. [32] and Tang et al. [33], respectively. The obtained hydrogels were casted onto transparent glass Petri dishes and then dried at 70 °C for 2 h [34]. Finally, different concentrations of curcumin (0.15, 0.3, and 0.6%, (wt./v)) were added portion-wise on CMC-Na/SA blends and agitated using harsh stirrer at 65 °C and 200 rpm for 20 min until obtaining completed dispersed solution. After that, $PdCl_2$ solution was added as previously mentioned until ideal curcumin-loaded hydrogel formation.

2.3 Physicochemical Measurements of CMC-Na/SA/$PdCl_2$ Composite Hydrogels

2.3.1 Gel Fraction (Gf %)

The gel fraction (%) of crosslinked hydrogel is the ratio of the dry gel weight (W_d) to the initial weight of the polymer (Wi) [35]. Samples were cut into specific dimensions (0.5 $\times$ 0.5 $\times$ 0.3 mm^3), allowed to dry to a consistent weight,

and then placed in distilled water (DW) for 3 days at 25 °C. The water was changed every single 24 h. After being thoroughly cleaned, the proposed hydrogels were allowed to dry for 2 days at room temperature before being placed at 40 °C in a vacuum oven to get consistent weight. The following formula was used to calculate the gel fraction (GF)%.

$$GF(\%) = (W_d/W_i) \times 100. \quad (1)$$

where W_d is the weight of the dry, insoluble portion of hydrogel following water extraction and W_i is the initial weight of the hydrogel [36].

2.3.2 Swelling (%)

Water uptake (%) or the swelling % of composite hydrogels was determined by assessing the hydrogel's capacity to absorb water or other physiological fluids in relation to time [37]. Distilled water was used to soak the membranes at 37 °C. Hydrogels were weighed separately at regular interval times. Swelling degree or water absorption (%) of hydrogels was determined using the following equation.

$$\text{Swelling}\,(\%) = \left(\frac{W_s - W_e}{W_e}\right) \times 100. \quad (2)$$

where the swollen weight sample is represented as W_s and dried sample weight after water-logged is represented as W_e [38].

2.3.3 Hydrolytic degradation

Membranes were submerged in distilled water to measure the hydrolytic degradation index of the hydrogels were calculated at 37 °C at interval times versus the weight loss (%), once the verified films reached the steadiness-swelling state by utilizing the provided formula.

$$\text{Weight loss}\,(\%) = \left(\frac{W_o - W_t}{W_o}\right) \times 100. \quad (3)$$

where the membrane original weight is represented as W_o, the membrane weight at specific incubation time is represented as W_t [31].

2.4 Characterization of Curcumin-Loaded and Unloaded CMC-Na/SA/$PdCl_2$ Composite Hydrogels

Samples preparation route and all instrumental characterization which were used for testing the prepared composite hydrogels, *e.g.*, FT-IR, XRD, SEM and TGA, were explained in detail in *Supplementary data*.

Table 1 List of formulations tested, along with their constituents and codes

Codes	Samples composition	Curcumin (Cr) concentrations (wt./v, %)
M1	CMC-Na:SA (4:1) + 0.4% $PdCl_2$	0
M2	CMC-Na:SA (4:1) + 0.4% $PdCl_2$ + Cr	0.15
M3	CMC-Na:SA (4:1) + 0.4% $PdCl_2$ + Cr	0.3
M4	CMC-Na:SA (4:1) + 0.4% $PdCl_2$ + Cr	0.6
M5	CMC-Na:SA (4:1) + Cr	0.15
M6	CMC-Na:SA (4:1) + Cr	0.3
M7	CMC-Na:SA (4:1) + Cr	0.6

2.5 Bio-evaluation of Curcumin Unloaded and Loaded CMC-Na/SA/ $PdCl_2$ Hydrogels

2.5.1 Safety Assay and Anticancer Activity

An in vitro cell viability test was carried out to assess the safety profile and the anticancer activity of tested samples on *WISH* cell line as a normal cell line and also on *Wi-38*, *CaCo-2, HepG-2* and *MDA-MB-231* as cancerous cell lines using MTs assay (*Promega*) according to the manual instructions. Before the day of the experiment, 1 mL of 6×10^3 cells/ml of the precultured cells was inoculated into 12-well plates, and then the plates were incubated overnight till semi-confluence. After cells semi-confluence, the exhausted media were removed and replaced with new culture media, and then, the pre-sterilized membrane using UV for 3 h cubic pieces (2 cm × 2 cm) were added to the plate wells. After two days of incubation, the cellular viability and cytotoxicity (%) were calculated by quantifying the solubilized formazan in DMSO at 570 nm.

2.5.2 Antimicrobial Bioassays

The antimicrobial effectiveness of the formulations under investigation was estimated in the sections that followed utilizing a range of methods, such as inhibition zones diameters, turbidity readings, and biofilm inhibition assay.

2.5.2.1 Measurement of Inhibition Zone Diameters The antimicrobial activities of the tested formulations that coded in Table 1 were evaluated using the agar well-diffusion assay [39] against multidrug-resistant human pathogens

including *Salmonella paratyphi, Escherichia coli,* and *Pseudomonas aeruginosa* (*Gram*-negative bacteria), *Staphylococcus epidermidis, Staphylococcus aureus*, and *Bacillus cereus* (*Gram*-positive bacteria), and *Candida krusei, Candida tropical,* and *Candida glabrata* (yeast cells). Microbial inoculum was initially grown on nutrient broth medium, which was prepared by mixing (0.5 g peptone, 1.5 g beef extract, 1.5 g yeast extract, and 0.5 g sodium chloride in 100 ml of DW). On the one hand, the culture suspensions were prepared by diluting microbial grown cells with 0.85% saline (w/v) using a *McFarland No.1* standard (3×10^8 CFU/ml) [40].

On the other hand, 50 ml of sterile nutrient agar medium was poured into sterile petri plates (140 mm in diameter) and allowed to solidify. Following that, 100 µl of each prepared microbial inoculum was spread uniformly on the plates with sterile plating swab spreaders. The inoculated petri dishes were left for 1 h to allow the pathogen to properly absorb into the medium. Using a sterile cork borer, wells (7 mm in diameter) were aseptically drilled in the inoculated medium. The prepared wells were filled with 80 µl of the test formulae, and the plates were left at 4 °C for 4 h to allow for diffusion. These plates were then kept for 24–48 h at 37 °C. Therefore, a scientific region ruler was used to measure the diameter for any zones of inhibition observed on the plates. The antimicrobial efficiency of the tested formula was then calculated using the width differences between the visible inhibition zones surrounding the wells. Larger inhibition zones are strongly associated with higher antimicrobial activity. Technical and biological test replicas were carried out triplicated.

2.5.2.2 Evaluation of the Microbial Inhibitory Rate In brief, tested human pathogens were cultured in nutrient broth at 37 °C and 200 rpm until exponential growth began. The diluted microbial cultures (a concentration of (0.2×10^8) CFU/ml corresponding to an optical density OD_{600nm} of 0.3) were then treated with various formulations for 24 h at 37 °C in glass culture tubes. The resulting turbidity was measured after incubation by measuring the optical density at 600 nm [39, 41]. Finally, the percentages of microbial growth inhibition were calculated. This assay was carried out three times in separate experiments for each of the tested pathogens.

2.5.2.3 Biofilm Inhibitory Assay For this assay, sterile glass test tubes contained 4.5 ml of microbial culture (3×10^7 CFU/ml) that was mixed with 500 µl of the tested formula and then incubated for 24 h at 37 °C and 200 rpm. Following incubation, the spread plate method was used to swab 100 µl of each diluted culture in solid nutrient agar medium in order to count the biofilm-forming colonies in each replicate ($n = 3$). Colony-forming units per milliliter (CFU/ml) were used to tabulate the results. To determine the level of biofilm inhibition, the logarithm reductions of the pathogen's cells exposed to various formulations were computed [39, 42, 43]. The calculated biofilm inhibition was evaluated using untreated control tubes (100% cell growth) and medium control tubes (0% cell growth) to determine the efficiency of the antimicrobial efficacy.

2.6 Statistical Analysis

Each experiment was repeated at least three times. All values were informed by the mean and standard deviation ($M \pm SD$). Statistical analysis was conducted using *Minitab 18* software, which included a one-way analysis of variance. *Tukey's* test values were considered significant, as probability values were less than 0.05 ($P < 0.05$).

3 Results and Discussion

3.1 Gel Fraction

CMC-Na/SA/$PdCl_2$ composite hydrogels were prepared by ionic gelation method. In this process, anionic carboxylic groups existing in SA and CMC interact with bivalent palladium ion (Pd^{2+}) to form the gel [32]. The results show that three hours for $PdCl_2$ dispersion could be needed since the more sonication time produces greater dispersion of $PdCl_2$ particles and therefore further crosslinking effect is obtained. This is noticed by preparing CMC-Na/SA/$PdCl_2$ hydrogels with different dispersion times of $PdCl_2$ (0.5, 1, and 3 h). It was observed that 0.5 h of $PdCl_2$ dispersion produced faint brownish yellow color producing a partial gelation, while 1 and 3 h of dispersion times produce light brown and dark brown color, respectively, giving complete crosslinked hydrogels. $PdCl_2$ is added as a dispersed solution into CMC-Na/SA blend solution not as crystals due to it being aggregated on the surface of the blend and cannot make the polymers-blend solution crosslinked. These concentrations of 2% SA and 2% CMC-Na solution have been selected because 4 wt.% of both polymer solution is very viscous solution hindering the crosslinking process.

It was found that the needle is the preferable choice for the addition of $PdCl_2$ solution as the addition of $PdCl_2$ solution dropwise without a needle on the surface of blended polymer solutions made rapid gel formation on the surface. Figure 1a elucidates that gel fraction increases with rising the ratio of CMC-Na, since CMC-Na:SA (4:1) and CMC-Na:SA (2:1) in the formula CMC-Na/SA/0.4%$PdCl_2$ produced GF % approximately 91% and 89%, respectively, because the highest crosslinking degree is obtained by increasing the CMC-Na content. However, GF% decreases to be 74% by increasing the SA content that is reliable with previous obtained findings of Ibrahim et al. [34]. Figure 1b indicates that GF% elevates with increasing of $PdCl_2$ ionic crosslinker.

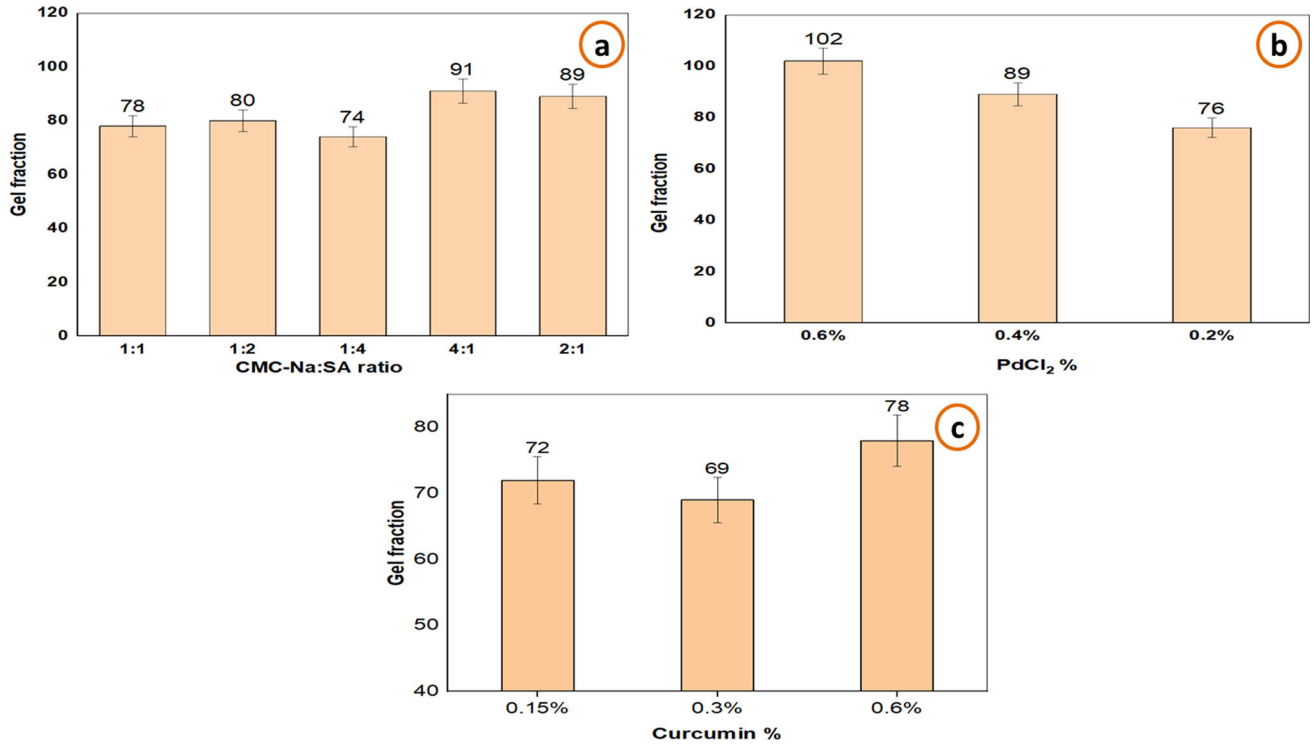

Fig. 1 Gel fraction (%) of formed composite hydrogels; **a** Different ratios of CMC-Na:SA at 0.4% of $PdCl_2$, **b** Different concentrations of $PdCl_2$ and Na-CMC:SA (4:1), and **c** Different concentrations of curcumin loading at 0.4% $PdCl_2$ and Na-CMC:SA (4:1)

Figure 1b shows that the resulted GFs% of crosslinked CMC-Na:SA (4:1) are 102, 89, and 76% at 0.6, 0.4, and 0.2% of $PdCl_2$, respectively; however, at 0.1% $PdCl_2$ no gel formed. Figure 1c shows the effect of curcumin loading on gel fraction. It is observed that the addition of curcumin into hydrogel membranes reduced the formed gel fraction to a certain limit at which any increase in the concentration of $PdCl_2$ resulted in higher gel fraction. The resulted gel fractions of crosslinked curcumin-loaded CMC-Na:SA (4:1) $PdCl_2$ 0.4% are 72, 69, and 78% at 0.15, 0.3, and 0.6% of curcumin, respectively.

3.2 Swelling Study

The swelling ratio of all fabricated hydrogels was determined as shown in Fig. 2. Results demonstrate that swelling (%) estimates of all hydrogels induce gradually with expanding swelling time till accomplishment of the equilibrium swelling phase after 72 h. The first state of equilibrium swelling is settled and arranged after 36 h for CMC-Na:SA (1:1), 48 h for CMC-Na:SA (2:1), 72 h for CMC-Na:SA (1:2), CMC-Na:SA (1:4), and 96 h for CMC-Na:SA (4:1). As shown in Fig. 2a, the highest swollen formula is CMC-Na:SA (4:1), which recorded a swelling % ~ 2900%, while the least swelling % obtained for CMC-Na:SA (1:4) is around 835%. It is indicated that the swelling (%) increases with rising of CMC-Na contents in hydrogel components, which is ascribed to the abundance of greatly hydrophilic –OH and $COOCH_3$ groups of CMC-Na, where they enhance the affinity of hydrogels network to water molecules. The result of swelling is coupled with the results of Dai et al. who made a comparison between ionic crosslinked hydrogels of gelatin/sodium alginate (GL/SA, 4:1.6) prepared with no addition of CMC secluded from pineapple peel, representing that the blending of CMC into the hydrogels can improve the swelling capability [44]. The swelling can be justified by the statement that at the pH 7 of the swelling surrounding, the ratio COO^-/COONa of CMC-Na and SA rises because of improving ionization of carboxylic groups (COO). The network quickly relaxes as a result of these anionic electric centers resisting each other resulting in a rise in swelling % [45].

Sharp swelling is observed significantly at high concentrations of CMC-Na, compared to low concentration in (CMC-Na:SA 1:4) and (CMC-Na:SA 1:2) which recorded swelling % ~ 600 and 800%, respectively. This may be attributed to occurrence of termination reaction and complete consuming of crosslinking moieties, *i.e.,* (COO^-) between Pd and SA. Thus, it induces a simple participation of CMC-Na with crosslinking moieties, where $PdCl_2$ is pretended to perform as complexing carboxylate anions of methylcellulose and alginate by its divalent palladium ion (Pd^{+2}). Interestingly, the role of crosslinker degree on swelling ratio

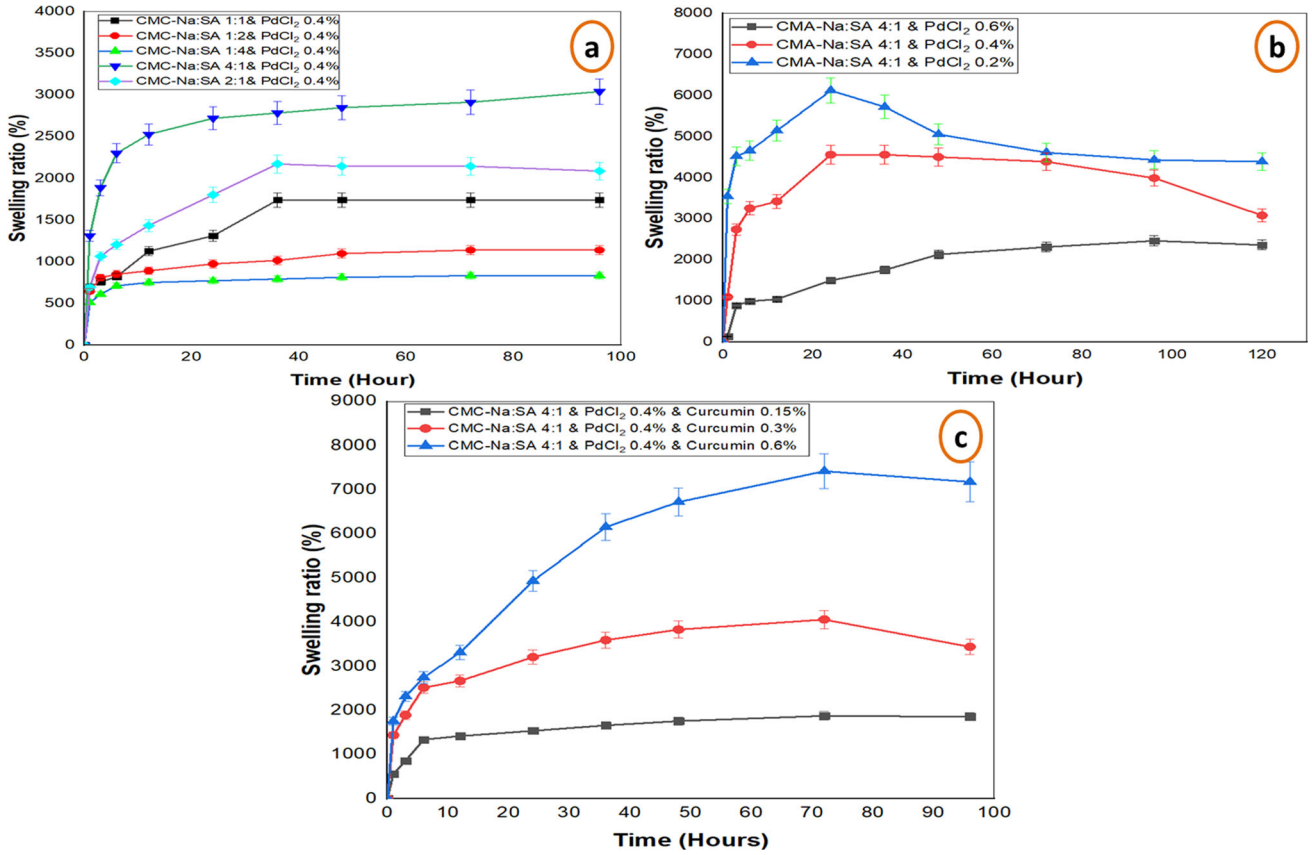

Fig. 2 Swelling ratio (%) of tested composite hydrogels: **a** Different ratios of CMC-Na:SA at 0.4% of $PdCl_2$, **b** Different concentrations of $PdCl_2$ and CMC-Na:SA (4:1), and **c** Different concentrations of curcumin loading at 0.4% $PdCl_2$ and CMC-Na:SA (4:1)

(%) of blended (CMC-Na:SA, 4:1) has been studied by varying the concentration of $PdCl_2$ in the range (0.2, 0.4, and 0.6%). Figure 2b demonstrates that swelling ratio reduces with rising concentration of $PdCl_2$. Accordingly, it is found that 0.4% $PdCl_2$ gives a proper swelling %, especially regarding the handling of the sample. As known, with increasing $PdCl_2$ concentration, the amount of Pd^{2+} ion per unit volume of the liquid increases and more Pd^{2+} could bond to the copolymer chains. This resulted in a diminished network space, so a smaller amount of water can enter the beads core. Meanwhile, $–COO^-$ groups decreased and consumed due to the combination of Pd^{2+} and –COOH groups of SA and CMC-Na. Thus, the electrostatic repulsion between $–COO^-$ groups converts weak, giving rise to the decrease of swelling (%) of hydrogels. In brief, 0.4% and 0.6% of $PdCl_2$ solution produced hydrogels with complete crosslinking and good mechanical properties. Although 0.2% of $PdCl_2$ produced partially crosslinked hydrogel with very low mechanical properties, 0.1% of $PdCl_2$ solution recorded no gel formed. This explanation couples with Ibrahim et al. who crosslinked alginate/CMC beads with $CaCl_2$ as a crosslinker [45].

The curcumin grafting into CMC-Na/SA scaffold reduced the crosslinking density of membranes, due to the non-miscible state formed as shown in Fig. 2c. This decreasing perhaps arise from the hydrophobic feature of curcumin which made it incompatible with other membrane components and thus this resulted in increment of the water capability and facilities the diffusion of water inside the membrane [46]. The impact of curcumin concentration on swelling ratio of different hydrogels has been investigated by altering the concentration of curcumin in the range (0.15, 0.3, and 0.6%). The results demonstrate that swelling % increases with increasing concentration of curcumin. It is found that membranes with less concentration of curcumin (0.15%) showed less swelling capacity unlike membranes with a higher concentration of curcumin (0.6%) showed higher swelling capacity.

3.3 Hydrolytic Degradation

It is found that the weight loss of composite hydrogels rises with increasing the ratios of SA (Fig. 3a). Here, the degree of ionization of carboxylate groups in SA improves which creates high number of carboxylate ions (COO^-) beside SA

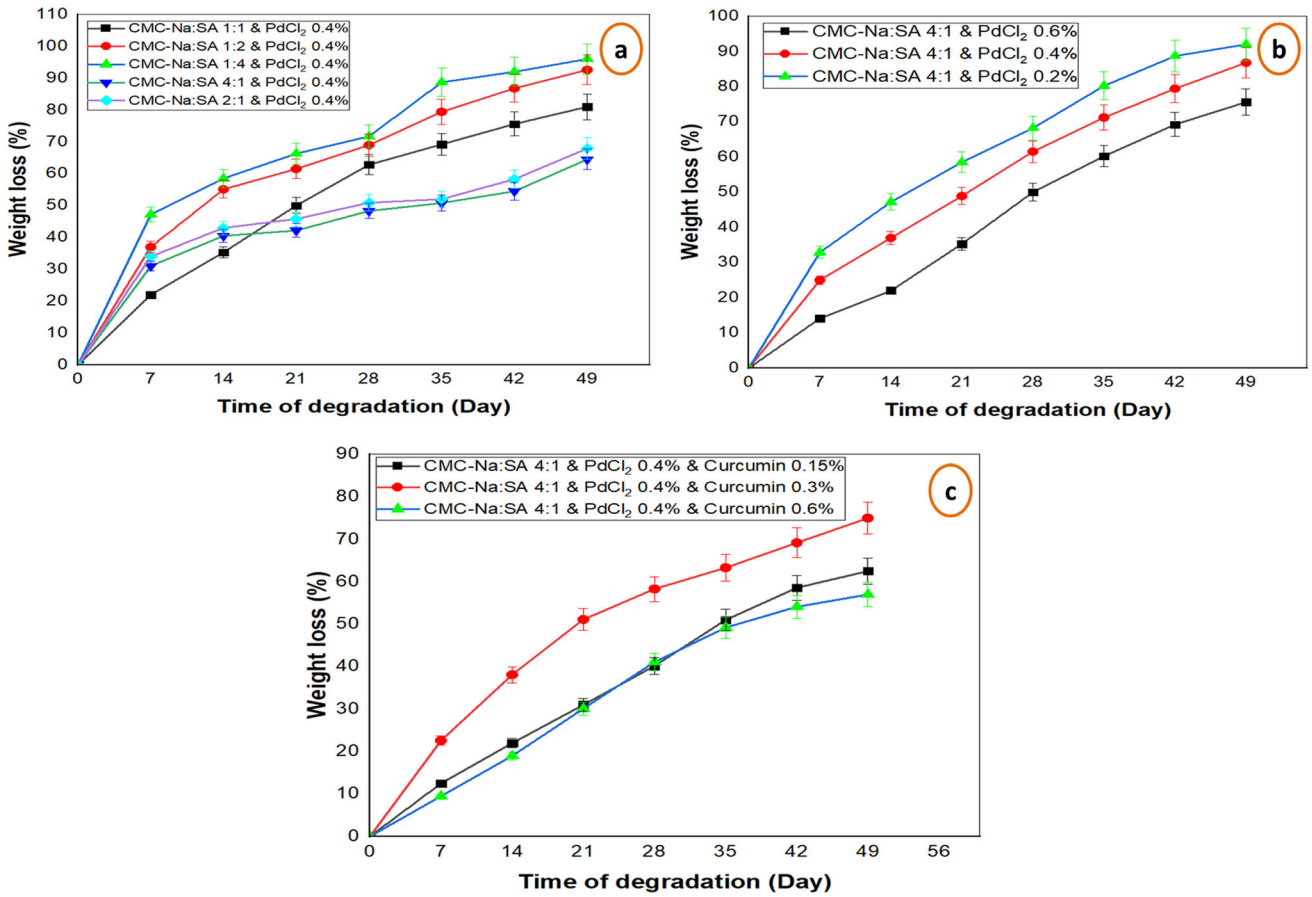

Fig. 3 Weight loss (%) of tested composite hydrogels: **a** Different ratios of CMC-Na:SA at 0.4% of $PdCl_2$, **b** Different concentrations of $PdCl_2$ and CMC-Na:SA (4:1), and **c** Different concentrations of curcumin loading at 0.4% $PdCl_2$ and CMC-Na:SA (4:1)

moieties. These ions of anionic charged carboxylate disgust each other and result in a fast moderation in the network. That obviously resulted in an increment in weight loss (%). Figure 3b shows the impact of different concentrations of $PdCl_2$ on degradation rate of composite hydrogels when placed in deionized water for a specified period**.** As seen, hydrogels crosslinked with 0.2% $PdCl_2$ show weight loss approximately 92%, while other hydrogels crosslinked with 0.4% $PdCl_2$ display weight loss approximately 75.6% in the seventh week. The test records that the more $PdCl_2$ content gave the less weight loss of hydrogel. Figure 3c illustrates the effect of loading curcumin on weight loss of hydrogels, where the degradation rate increases with high concentration of curcumin to a certain limit at which the degradation rate decreases, as shown at 0.6% curcumin. This may be attributed to immiscible phase formed due to hydrophobic nature of curcumin which resulted in reduction of crosslinking density of hydrogels and then facilitating the penetration of water within hydrogel networks [46].

3.4 FT-IR Assessment

Figure 4 displays the spectra of different prepared CMC-Na/SA composite hydrogels. It is obviously recorded that for SA and CMC-Na, the wide-ranging peaks at ν 3323, 3373 cm^{-1}, respectively, are related to (–OH) stretching vibration, but the characteristic peak of –OH group is resulting from blinding of SA and CMC-Na, which is detected at ν 3419 cm^{-1}. This obvious change is owing to the formation of hydrogen bonds linking of CMC-Na and SA. The main peak of metallic bond (Pd–o) was recorded at ν 620 cm^{-1} in crosslinked CMC-Na and at ν 616, 708 cm^{-1} in crosslinked SA [47], while the appearance of a shoulder peaks at ν 2908 cm^{-1}, 2920 cm^{-1} is assigned to –CH stretching vibration. A meaningful stretching C–O vibration of primary ethers and alcohols in cellulose backbone is observed at ν 1023 cm^{-1}.

FT-IR spectra of CMC-Na or SA and CMC-Pd or SA-Pd hydrogel do not significantly differ from one another, and no additional peak could be seen in CMC-Na/SA composite hydrogel. This observation might be because of the truth that the crosslinking includes the replacement of Na^{1+} with Pd^{2+}

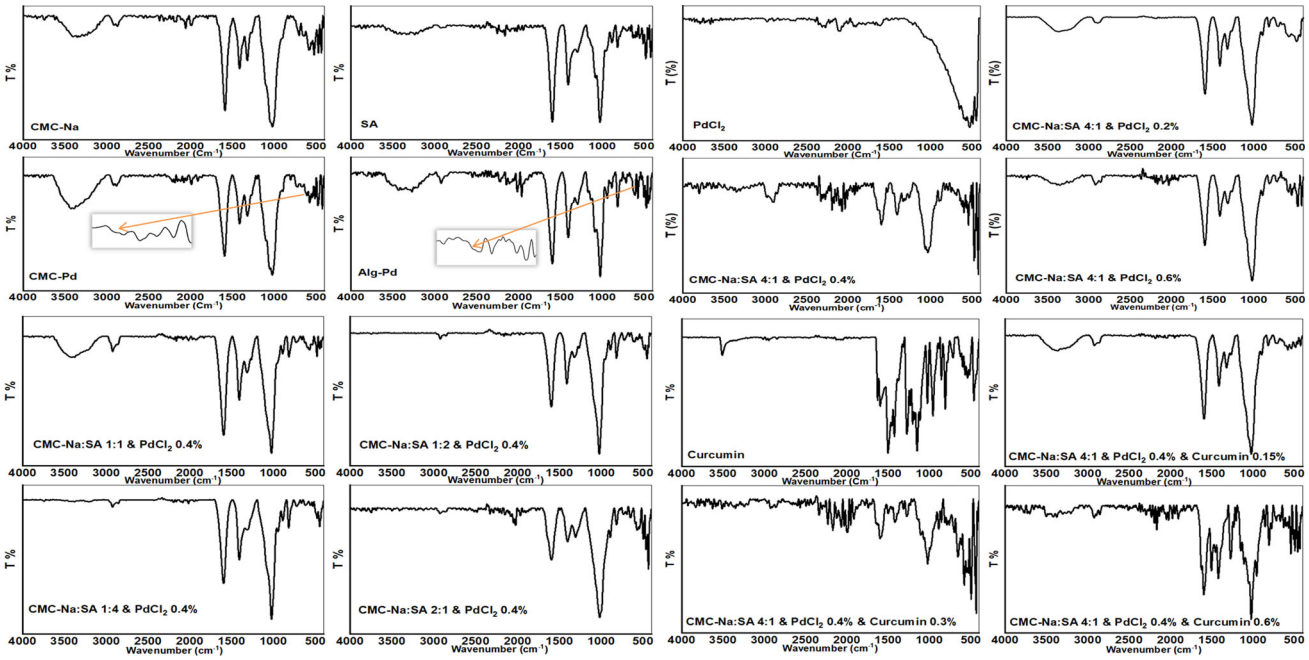

Fig. 4 FT-IR spectra for CMC-Na, SA, $PdCl_2$, curcumin-loaded and unloaded composite hydrogels

derived from $PdCl_2$. The bidentate of the carboxylate group to Pd^{2+} very slightly changed the wavenumber once Pd^{2+} ionic linking in Na-CMC/SA chain from ν 3350 cm^{-1} to a higher ν 3418 and 1413 cm^{-1} and peak shifted to ν 1403 cm^{-1} [48].

In SA and CMC-Na hydrogels, peak of C–C stretching ν 1028 cm^{-1} is more intense, pointing to either a stronger O–H binding vibration or a stronger binding of Pd^{2+} to carboxylate group [49]. The peak breadth of hydroxyl (OH) stretching vibration initially grew, then reduced, and accomplished its maximum at CMC-Na:SA (4:1) as CMC-Na content is increased. The ($–COO^-$) antisymmetric stretching peaks of CMC-Na and SA are the absorption peaks near at ν 1588 and 1598 cm^{-1}, respectively. However, in CMC-Na/SA blend, the intensity and position of the $–COO^-$ antisymmetric stretching absorption peak are near ν 1592 cm^{-1} which also has a lower shift, and the intensity changes of all blends have little difference and decrease successively. Hydrogel formulas (CMC-Na:SA, 2:1) and (CMC-Na:SA, 4:1) experience smaller intensity at -COO- antisymmetric stretching vibration peak than other groups.

Moreover, in SA and CMC-Na, the vibration peak over ν 1417 cm^{-1} is a $–COO^-$ symmetric stretching peak, while the vibration band near ν 1324 cm^{-1} is a -OH bending peak. The vibration band of the CMC-Na/SA composite hydrogel at ν 1312 cm^{-1} rises, and the regarding strength is higher than that at ν 1410 cm^{-1} ($–COO^-$ symmetric vibration band was lifted from ν1417 cm^{-1}). That is due to the formation of hydrogen bonds formed by the –OH and $–COO^-$ in CMC-Na and SA in addition to the crosslinking activity of $PdCl_2$. These aspects increase the symmetric stretching absorption of $–COO^-$ and decrease the bending absorption of –OH. Additionally, compared to the CMC-Na, both peaks have lower intensities following the ionic crosslinking, which illustrate hydrogel's loss of its crystallinity especially in CMC-Na/SA (4:1 and 2:1) hydrogels. Similarly, the intensity change initially increases and then decreases with the rise of CMC-Na quantity in CMC-Na/SA. It is clear that CMC-Na/SA (4:1) has a higher intensity than CMC-Na/SA (1:1), CMC-Na/SA (1:2), CMC-Na/SA (1:4), and CMC-Na/SA (1:2) at ν 1422 cm^{-1}, and CMC-Na/SA 1:4 has the greatest intensity fluctuation [23].

The spectrum of curcumin displays a vibration peak at ν 3510 cm^{-1} marks to the stretching substitution of phenolic group. Moreover, sharp vibration peaks ranged from ν1450 to 1630 cm^{-1} corresponding separately to groups C=O,–OH, and C=C (enol) [50]. Because of the aromatic vibrations of the benzoate groups and aromatic C–H, extra two peaks of about ν 713 and 950 cm^{-1} are discovered after embedding of curcumin into the fabricated membranes. This theory supports the fact that curcumin is loaded onto hydrogel. Additionally, the band's intensity is seen to be diminishing around about ν 1600 cm^{-1}. Additionally, a peak that corresponds to O–H (between ν 3600 and 3000 cm^{-1}) is shrunk and moved from wave number ν 3398 to 3356 cm^{-1}. Notably, the peak at ν 2919 cm^{-1} in SA/CMC-Na/Cr exhibits distinct intensity compared to unloaded SA/CMC-Na. This is described by the creation of hydrogen bond inter-molecularly between membrane components and curcumin [31] as shown in Fig. 4.

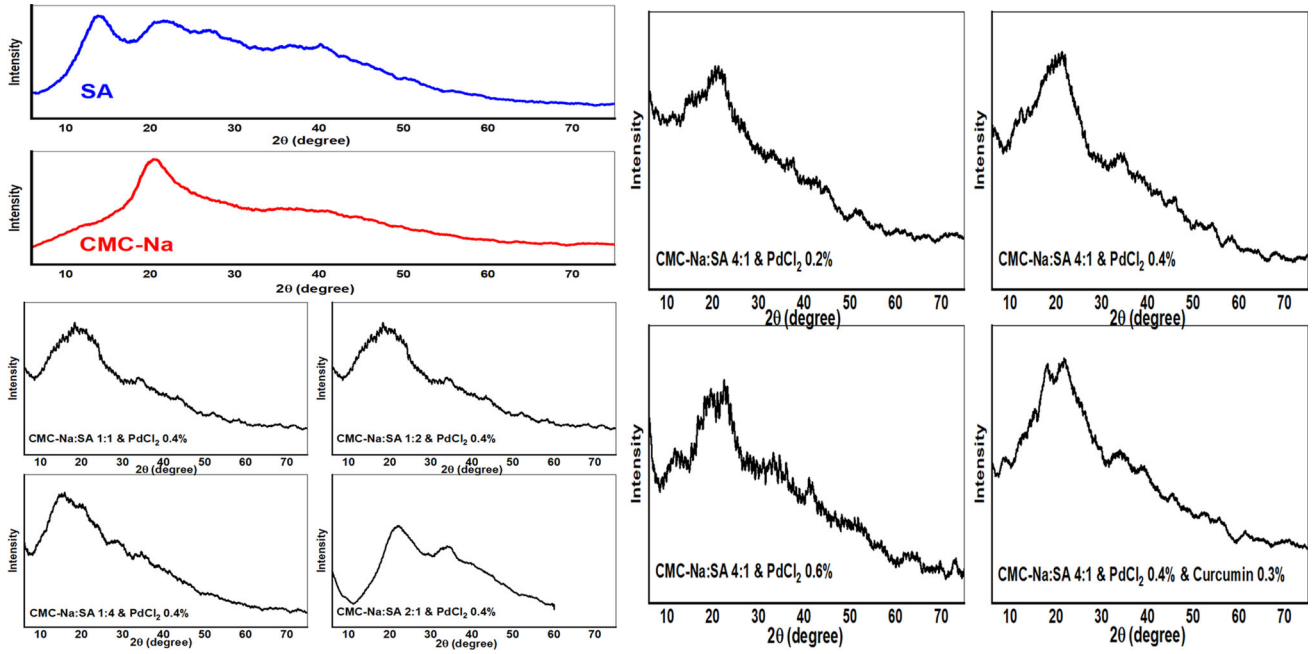

Fig. 5 X-ray diffraction patterns of CMC-Na, SA, and different Cr-loaded CMC-Na/SA/$PdCl_2$ composite hydrogels

3.5 XRD Investigation

Figure 5 displays XRD spectra of CMC-Na/SA blended hydrogels. IXRD pattern of pure SA demonstrates characteristic peaks at $2\theta = 13.9°$ and 21.7°, respectively [51], while the diffractogram of pure CMC-Na consisted of a broad characteristic peak at $2\theta = 20.5°$, indicating that its structure is amorphous. Aforementioned, three characteristics peaks corresponding to SA and CMC are all present in XRD profile of CMC-Na/SA hydrogel membranes. However, the peaks are broadened showing increasing the amorphous nature of formulations [32]. Meanwhile, diffractogram of different compositions of CMC-Na/SA hydrogels exhibits the broadband at different values of 2θ, where it is recorded at $2\theta = 18.3°$ for CMC-Na:SA (1:1), CMC-Na:SA (1:2), $2\theta = 15.4°$ for CMC-Na:SA (1:4), $2\theta = 20.5°$ for CMC-Na:SA (4:1), and $2\theta = 22°$ for CMC-Na:SA (2:1). It can be attenuated to the amorphous halo state of the polysaccharides of CMC-Na and SA [52]. Also, Fig. 5 shows a handful of peaks ranged at $2\theta = 10°$ to 30°, albeit they are not particularly visible. These peaks show that the matrix contains extremely crystalline curcumin [53].

3.6 TGA Results

TGA is performed to investigate the degradation and thermal stability of three formulas of crosslinked CMC-Na/SA (4:1) with different concentrations of $PdCl_2$ (0.2, 0.4, and 0.6%), as shown in Fig. 6. TGA thermographs exhibit a stepwise and consecutive weight loss patterns. Basically, the thermal decomposition process of hydrogels could be mostly divided into four stages. The first thermal decomposition is associated with all samples attributed to loss of adsorbed water, humidity or solvents traces, where the weight loss observed is ~ 15%, 12%, and 13% in the temperature range of 28–190 °C for hydrogels crosslinked with (0.6, 0.4, and 0.2) $PdCl_2$, respectively. The second decomposition stage is detected at 228–305 °C, where weight loss is found 38%, 40%, and 38% was recorded in hydrogels with 0.6, 0.4, and 0.2 $PdCl_2$, respectively; this weight reduction is regarded to breakdown of glyosidic bonds. At this stage, approximately 40% of the tested sample stayed and corresponded to intermediate carbonaceous char material. In addition, the weight loss of about 6.1%, 6% and 6.6% is monitored between 305 and 500 °C, which is associated with oxidation of previously formed intermediate carbonaceous char material [54]. According to Kang et al., the main weight loss is detected ~ 257–300 °C and the further weight loss from 300 to 550 °C both corresponded to the decomposition of oxygen-containing groups like carboxyl and hydroxyl groups [55]. The superior thermal stability observed in hydrogel with the lowest concentration of palladium (II) ions is likely from effective crosslinking of hydrogel membrane owing to good diffusion of Pd^{2+} into the CMC-Na/SA membrane during formulation [54].

3.7 SEM Investigation

SEM cross-sectional investigation is always developed to provide the insight of topographical data and structural characteristics of hydrogels. Figure 7 shows the morphological

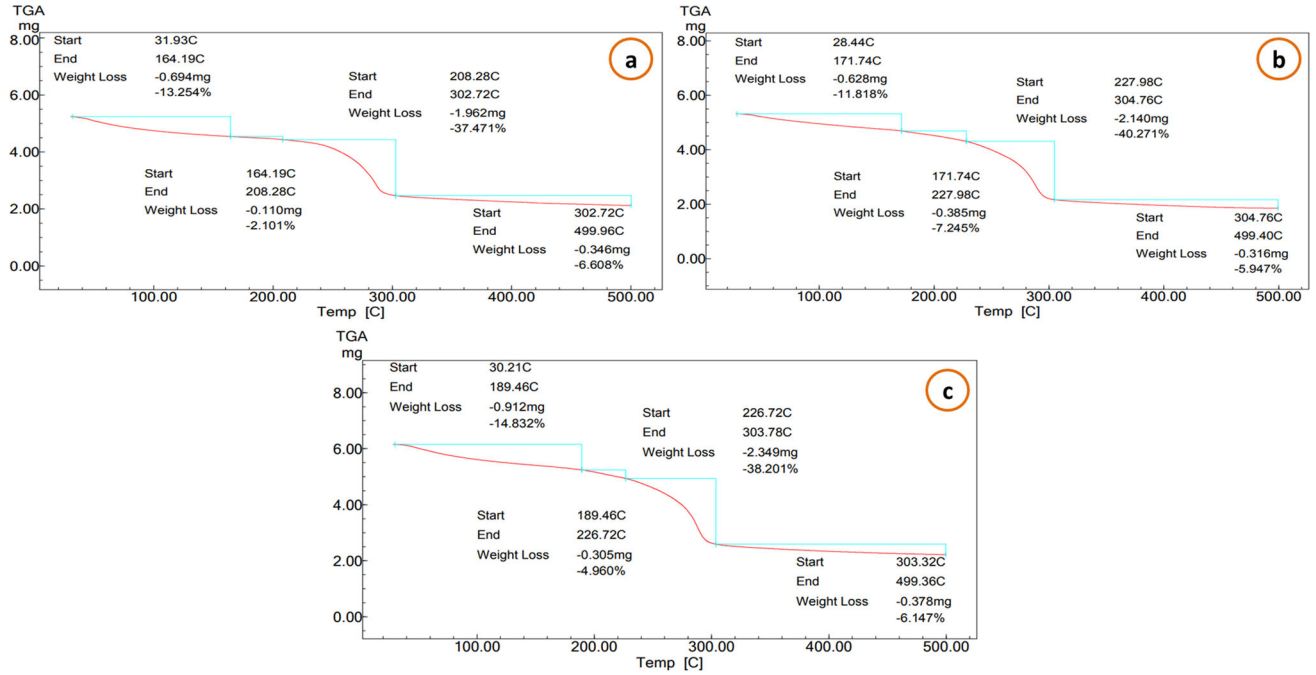

Fig. 6 TGA thermographs of Cr-loaded CMC-Na/SA/$PdCl_2$ composite hydrogels with different concentrations of $PdCl_2$; (0.2, 0.4, and 0.6 wt./v, %) (**a**, **b** and **c**) respectively

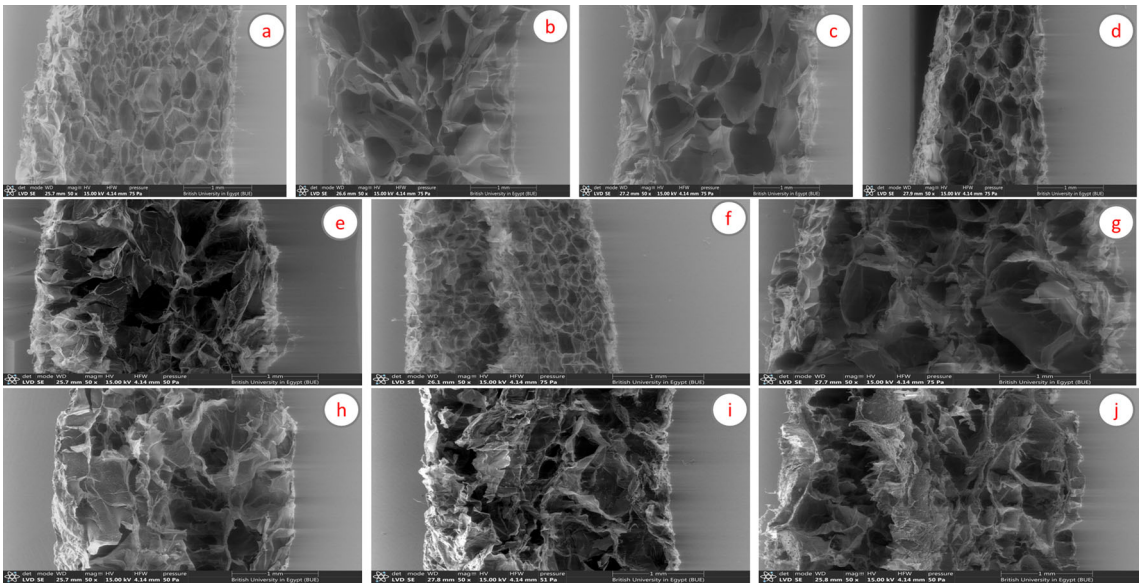

Fig. 7 SEM images of different Cr-loaded CMC-Na/SA/$PdCl_2$ composite hydrogels, **a** CMC-Na:SA (1:1)/$PdCl_2$ 0.4%, **b** CMC-Na:SA (1:2)/$PdCl_2$ 0.4%, **c** CMC-Na:SA (1:4)/$PdCl_2$ 0.4%, **d** CMC-Na:SA (2:1)/$PdCl_2$ 0.4%, **e** CMC-Na:SA (4:1)/$PdCl_2$ 0.2%, **f** CMC-Na:SA (4:1)/$PdCl_2$ 0.4%, **g** CMC-Na:SA (4:1)/$PdCl_2$ 0.6%, **h** CMC-Na:SA (4:1)/$PdCl_2$ 0.4%/Cr 0.15%, **i** CMC-Na:SA (4:1)/$PdCl_2$ 0.4%/ Cr 0.3%, and **(j)** CMC-Na:SA (4:1)/$PdCl_2$ 0.4%/ Cr 0.6%

features of different composition of hydrogels and porosity distribution. It is observed that the regular with good distribution of porous is observed by increasing the concentration of CMC-Na, as shown in Fig. 7a, d, e, and f, while Fig. 7b and c shows big porous with irregular cross-sectional structure according to high concentration of SA in hydrogel composition. After adding the curcumin, the structure of hydrogels turned to the fluffy structure with lower porosity as shown in Fig. 7h, i, and j.

3.8 Cytotoxicity Test

The cytotoxic activity of standard materials (e.g., $PdCl_2$, Cr, CMC-Na, SA) and different hydrogel formulas (CMC:SA (1:1)/$PdCl_2$ 0.4%, CMC:SA (1:2)/$PdCl_2$ 0.4%, CMC:SA (1:4)/ $PdCl_2$ 0.4%, CMC:SA (4:1)/$PdCl_2$ 0.4%, and CMC:SA (2:1)/$PdCl_2$ 0.4%), with different concentrations of $PdCl_2$ (CMC:SA (4:1)/$PdCl_2$ 0.6% and CMC:SA(4:1)/$PdCl_2$ 0.2%) and with different concentrations of loaded curcumin (CMC:SA (4:1)/$PdCl_2$ 0.4%/0.15% Cr, CMC:SA (4:1)/$PdCl_2$ 0.4%/0.3% Cr, and CMC:SA (4:1)/$PdCl_2$ 0.4%/0.6% Cr) are assessed against three carcinoma cell lines (e.g., human hepatocellular carcinoma *HePG-2*, human colon carcinoma *CaCO-2*, and human breast cancer *MDA-MB231)* and diploid human cell line composed of fibroblasts derived from lung tissue of a 3-month-gestation female fetus *Wi-38* cell lines using colorimetric MTT-assay in vitro at 2 days' time intervals. IC_{50} (the concentration of test compounds required to kill 50% of cell population) is determined from the dose–response curve. The activity was expressed as IC_{50} values (mg/ml) ± SD from 3 replicates.

Results reveal that IC_{50} values for $PdCl_2$, Cr, CMC-Na, and SA that killed ~ 50% of *HePG-2* are 186, 170, 537.2, and 2323.8 mg/ml, of *MDA-MB231* are 675, 1940, 38,424.2, and 8.3×10^{10} mg/ml, of *CaCO-2* are 897, 1617.4, 12.5624×10^3, and 420.2912×10^3 mg/ml, and of *Wi-38* are 2374.76, 1546, 9433.8, and 30.4799×10^3 mg/ml, respectively, after 2 days of cell exposure, as shown in Fig. 8. From the previously determined IC_{50} values, it is observed that $PdCl_2$ is the most cytotoxic component in hydrogel against *HePG-2, CaCO-2,* and *MDA-MB231* cells in addition to its quite safe effect, compared to Cr on normal cells. Dose-based curves for experimented cell lines are displayed in Fig. 8. The mortality mechanism of $PdCl_2$ as anticancer agent can be explained by the fact that palladium compounds interact with DNA, induce apoptosis, and cause cell cycle arrest. They show high selectivity to oligonucleotide end regions and can enter into non-covalent, electrostatic, and hydrogen bonds with DNA. Additionally, they can upregulate Bax protein, downregulate Bcl-2 protein, and cause mitochondrial potential decrease, leading to apoptosis [56].

The results highlight that formulation with Cr-loaded crosslinked SA/CMC-Na exhibits significant inhibition of tumor death in vitro compared to Cr-free crosslinked SA/CMC-Na. This indicates that the cytotoxic capabilities of Cr-free hydrogel are significantly higher than the Cr-loaded hydrogel even at higher concentrations of Cr. This can be explained via the expected conflict between Pd ions and hydroxyl groups of Cr structure to bond with the carboxylate groups of SA and CMC-Na. It is also observed that sample coded: M1 (CMC:SA (4:1)/$PdCl_2$ 0.4%) is the most aggressive biomaterial toward *HePG-2*, since it increases the cytotoxicity to 80%, compared to 1.7% for control cell, indicating that M1 has the highest cytotoxic efficiency against *HePG-2* and the safest effect on normal human cell, as shown in Fig. 9 and Table 1. It is further evident that M4 (CMC:SA (4:1)/Pdcl2 0.4%/0.6% Cr) which contains 0.6% of curcumin possesses a lethal effect that does not exceed 50.5% for *HePG-2*, compared to 31.4% control cells which indicate marked cytotoxicity on human normal cell, as shown in Fig. 9. Moreover, it is noticed that S4 (CMC:SA (2:1)/$PdCl_2$ 0.4%) is the most formula that has cytotoxic effect toward *MDA-MB231* and *CaCO-2*, but it doesn't exceed 35% and 33%, respectively, compared to 6.5% for *Wi-38* cell which indicates its safe effect on normal human cell.

3.9 Antimicrobial Activities

Various methods including the estimation of inhibition zones, turbidity readings, and a biofilm inhibition assay are used to evaluate the antimicrobial efficacy of tested hydrogel formulations. The generated inhibitory zones are produced by applying these formulations against tested human pathogens that are screened (Fig. 10). Significantly, as indicated in Table 2, *Escherichia coli* appear the widest zone of inhibition (24.36 ± 3.49 mm) after exposure to M4 formula. Notably, none of pathogens under investigation showed any zone of inhibition when exposed to M7 formula, as shown in Table 2. Among *Gram*-positive bacteria, M3 formula produces the maximum inhibition zone (17.35 ± 4.21 mm) against *Staphylococcus epidermidis*. Furthermore, in yeast cell cases, none of formulae under examination showed any zone of inhibition against *Candida krusei*. Meanwhile, *Candida glabrata* indicate a low zone of inhibition (8.36 ± 3.01 mm) when exposed to M2 formula. The results of inhibitory zones assay are influenced by the formulation's toxicity, as well as the viscosity and the toxin's size-dependent diffusion ratio. So, to assess the direct interaction between human pathogens and the investigated formulation, macro-dilution bioassays were employed. In the experiments below, turbidity and biofilm inhibitory assays are applied to evaluate the antimicrobial activities of tested formulations against multidrug-resistant human pathogens [57]. Accordingly, the antimicrobial activities are evaluated by culturing pathogens loaded with those formulations alongside pathogens that were not loaded as a control.

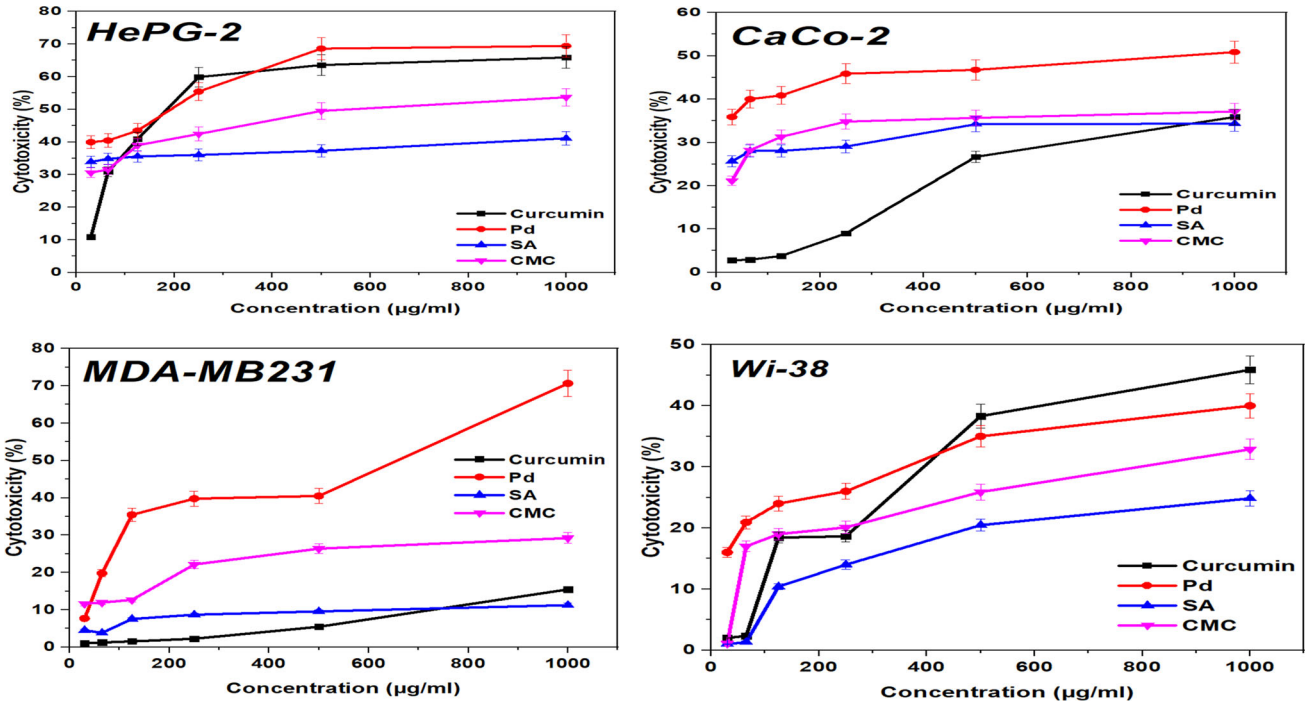

Fig. 8 Cytotoxicity (%) of curcumin, $PdCl_2$, SA and CMC-Na on *HePG-2*, *MDA-MB231*, *CaCo-2*, and *Wi-38* cells

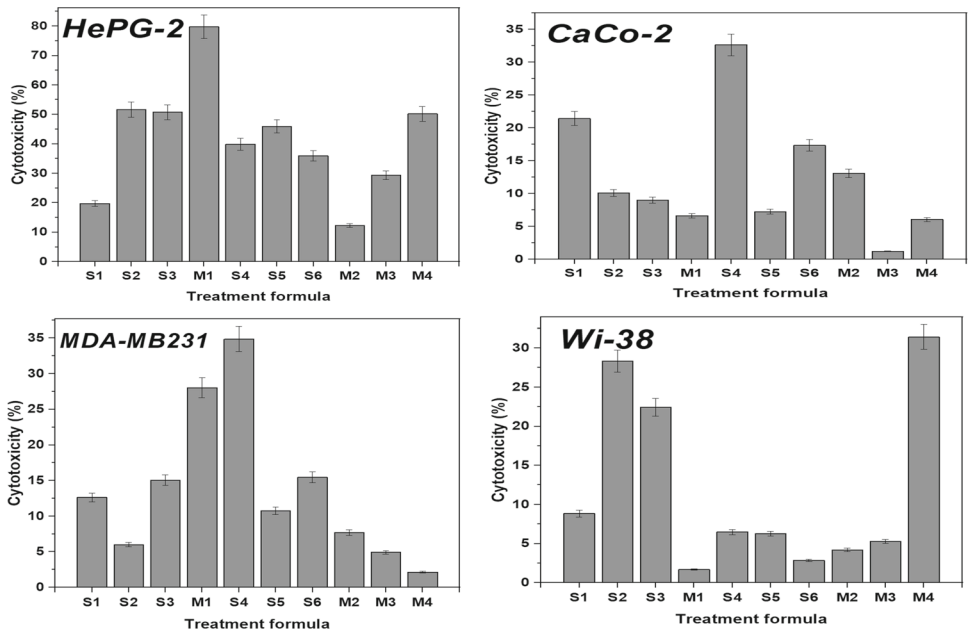

Fig. 9 Cytotoxicity (%) of different formulas on *HePG-2, MDA-MB231, CaCo-2*, and *Wi-38* cells. Here **S1**: CMC:SA (1:1)/$PdCl_2$ 0.4%, **S2**: CMC:SA (1:2)/$PdCl_2$ 0.4%, **S3**: CMC:SA (1:4)/$PdCl_2$ 0.4%, **M1**: CMC:SA (4:1)/$PdCl_2$ 0.4%, **S4**: CMC:SA (2:1)/$PdCl_2$ 0.4%, **S5**: CMC:SA (4:1)/$PdCl_2$ 0.6%, **S6**: CMC:SA (4:1)/$PdCl_2$ 0.2%, **M2**: CMC:SA (4:1)/$PdCl_2$ 0.4%/0.15% Cr, **M3**: CMC:SA (4:1)/$PdCl_2$ 0.4%/0.3% Cr, **M4**: CMC:SA (4:1)/$PdCl_2$ 0.4%/0.6% Cr

As shown in Table 3 and Fig. 11I, all tested formulations inhibited the growth of tested human pathogens significantly, compared to the optical densities produced by controls. The M4 formula significantly reduced the turbidity of all tested pathogens, with the strongest effects seen with *Staphylococcus epidermidis* ODs *ca.* (0.56 ± 0.02), *Bacillus cereus* (0.57 ± 0.35), and *Staphylococcus aureus* (0.98 ± 0.58), followed by *Pseudomonas aeruginosa* (0.92 ± 0.32). Notably, *Staphylococcus epidermidis* treated with M4 formula provided the lowest optical density because the control's optical density dropped sharply from 3.06 ± 0.014 to 0.56 ± 0.02. Besides, the optical density of control *Bacillus cereus* is sharply reduced from 3.09 ± 0.38 to 0.57 ± 0.35, nearly just like in the case of the M4-treated *Staphylococcus epidermidis*. Experts previously concluded that a palladium complex was linked via oxygen atoms of β-diketone group.

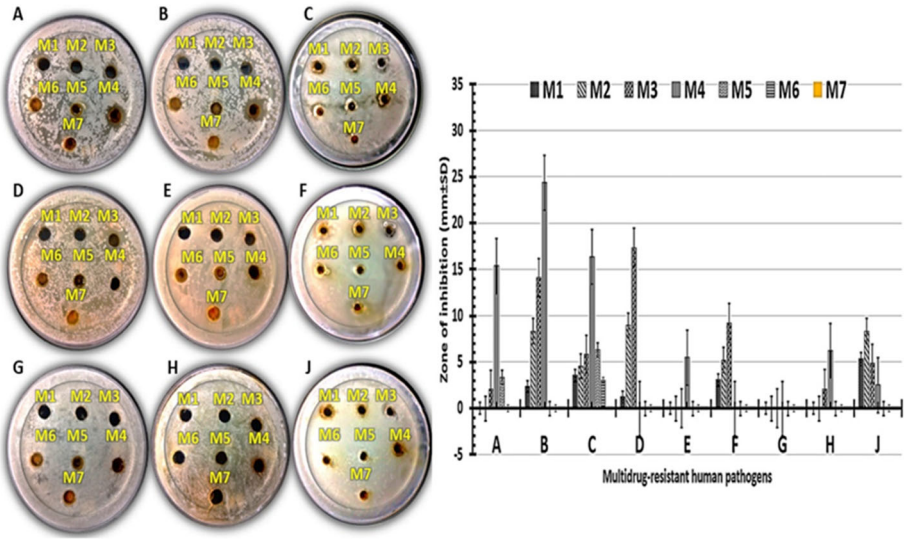

Fig. 10 Photos and histogram indicate the zone of inhibition (mm ± SE) against *Salmonella paratyphi* (**A**), *Escherichia coli* (**B**), *Pseudomonas aeruginosa* (**C**), *Staphylococcus epidermidis* (**D**), *Staphylococcus aureus* (**E**), *Bacillus cereus* (**F**), *Candida krusei* (**G**), *Candida tropicals* (**H**), and *Candida glabrata* (**J**)

Table 2 Formed inhibition zones of tested composite hydrogels against human pathogens

Multidrug-resistant human pathogens	Zone of inhibition (mm ± SD)						
	M1	M2	M3	M4	M5	M6	M7
Salmonella paratyphi	0	0	2.03 ± 0.36	15.36 ± 2.74	3.36 ± 0.98	0	0
Escherichia coli	2.36 ± .04	8.36 ± 1.64	14.12 ± 5.23	24.36 ± 3.49	0	0	0
Pseudomonas aeruginosa	3.56 ± 0.98	4.56 ± 2.84	5.84 ± 0.85	16.35 ± 0.36	6.35 ± 3.97	3.04 ± 1.54	0
Staphylococcus epidermidis	1.23 ± 0.05	8.94 ± 2.54	17.35 ± 4.21	0	0	0	0
Staphylococcus aureus	0	0	0	5.48 ± 1.24	0	0	0
Bacillus cereus	3.07 ± 0.07	5.23 ± 2.51	9.23 ± 0.09	0	0	0	0
Candida krusei	0	0	0	0	0	0	0
Candida tropicals	0	0	2.08 ± 0.07	6.23 ± 3.12	0	0	0
Candida glabrata	5.36 ± 3.47	8.36 ± 3.01	4.85 ± 2.08	2.51 ± 0.08	0	0	0

Accordingly, this structure, having a variety of biological properties, could be utilized as a powerful antimicrobial agent [58].

Various palladium (II) complexes have previously been explored as potential antibacterial agents. These complexes have also been shown to be more efficient against *Gram*-positive bacteria than *Gram*-negative bacteria [58]. As shown in Table 4 and Fig. 11II, the M4 formula significantly reduced the growth rate for all tested pathogens, but the strongest effects are seen against *Staphylococcus epidermidis, Bacillus cereus, and Staphylococcus aureus* (81.69 ± 9.34%, 81.55 ± 3.39%, and 78.50 ± 8.77%, respectively), followed by *Pseudomonas aeruginosa* (77.50 ± 6.11%), and *Escherichia coli* (72.75 ± 3.62%). The M4 formula (CMC-Na:SA 4:1/0.4% $PdCl_2$/0.6%Cr) has shown proficient antibacterial activity against all studied *Gram-positive* and *Gram-negative* bacteria, with the highest level of growth rate inhibition ranging from 81% (Table 4). However, in the case of yeast cells, *Candida krusei* is shown to have the highest inhibition percentage of growth rate (65.63 ± 8.76%), followed by *Candida glabrata* (62.42 ± 2.99%), and *Candida tropicals* (46.91 ± 3.58%). These results are validated by quantifying the CFU/ml and determining the percentage of biofilm inhibitory (Table 5 and Fig. 12). In general, there are no significant effects against all tested human pathogens among the tested M3, M5, and M6 formulas as shown in Table 5 and Fig. 12. Besides, the maximum biofilm inhibition % is recorded by M4 formula against *Staphylococcus aureus* (76.63 ± 2.43%), followed by *Bacillus cereus* (73.97 ± 6.82%) and *Candida krusei* (65.70 ± 3.72%). However, by using the same formula, the lowest biofilm inhibition is recorded against *Candida tropicals* (50.40 ± 6.28), and *Candida glabrata* (51.61 ± 3.45%), followed by *Salmonella paratyphi* (53.06 ± 1.94%), and *Escherichia coli* (56.70 ± 2.03%). In conclusion, M4 formula is more active in adjusting *Gram*-positive bacteria than *Gram-negative* bacteria or yeast cells. According to earlier studies, palladium and

Table 3 Measured turbidity (OD 600nm ± SD) of tested composite hydrogels against human pathogens

Multidrug-resistant human pathogens	Optical density (OD 600nm ± SD)							
	Control	M1	M2	M3	M4	M5	M6	M7
Salmonella paratyphi	1.36 ± 0.26a	1.19 ± 0.08a	1.13 ± 0.09ab	1.02 ± 0.09bc	0.85 ± 0.03c	0.91 ± 0.13c	0.99 ± 0.34c	0.95 ± 0.09c
Escherichia coli	3.45 ± 2.01a	3.09 ± 0.36a	2.32 ± 1.24ab	2.04 ± 0.08bc	0.94 ± 0.12c	1.04 ± 0.17c	1.12 ± 0.18c	1.16 ± 0.03c
Pseudomonas aeruginosa	4.09 ± 0.67a	3.98 ± 1.36a	3.04 ± 0.36ab	2.47 ± 0.91bc	0.92 ± 0.32c	1.19 ± 0.11c	1.28 ± 0.97c	1.28 ± 0.09c
Staphylococcus epidermidis	3.06 ± 0.01a	3.05 ± 1.25a	2.54 ± 1.25ab	0.96 ± 0.35bc	0.56 ± 0.02c	1.91 ± 0.54c	1.93 ± 1.67c	1.92 ± 0.94c
Staphylococcus aureus	4.56 ± 1.09a	3.37 ± 0.36a	2.21 ± 0.97ab	1.48 ± 0.01bc	0.980.58c	1.41 ± 0.67c	1.52 ± 0.34c	2.06 ± 1.07c
Bacillus cereus	3.09 ± 0.38a	3.02 ± 0.91a	2.89 ± 0.37ab	1.45 ± 0.34bc	0.57 ± 0.35c	1.09 ± 1.36c	1.16 ± 0.35c	1.18 ± 0.09c
Candida krusei	4.54 ± 1.98a	4.36 ± 1.36a	4.06 ± 0.97ab	2.23 ± 0.31bc	1.56 ± 0.97c	1.87 ± 0.31c	1.92 ± 0.03c	1.99 ± 1.09c
Candida tropicals	3.24 ± 2.07a	3.14 ± 0.97a	3.05 ± 2.09ab	2.97 ± 0.65bc	1.72 ± 0.19c	1.94 ± 0.91c	1.96 ± 0.92c	1.99 ± 1.07c
Candida glabrata	4.87 ± 1.72a	4.54 ± 3.12a	3.98 ± 0.97ab	3.54 ± 0.35bc	1.83 ± 0.97c	2.24 ± 1.34c	2.29 ± 0.96c	2.39 ± 0.38c

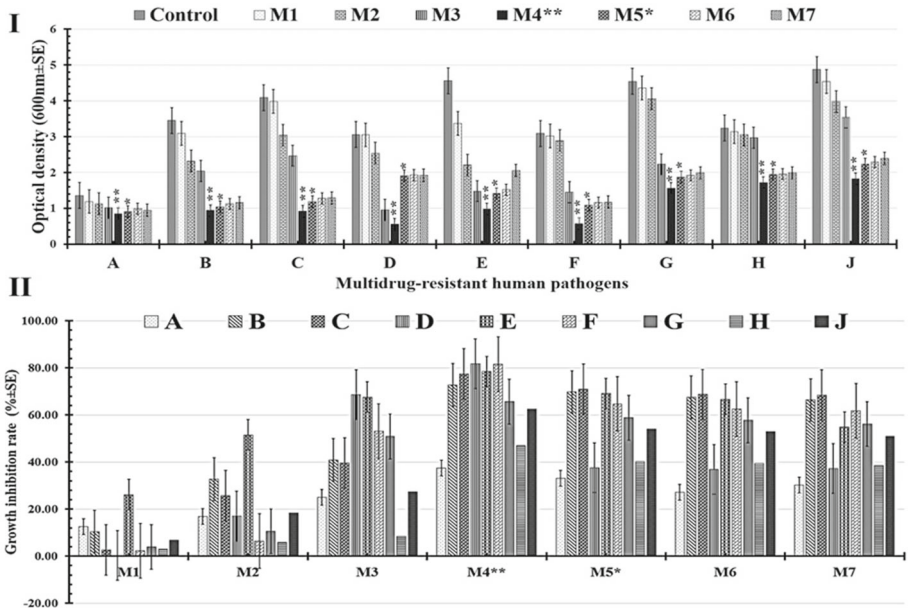

Fig. 11 Histograms of the measured turbidity ($OD_{600nm} \pm SE$) **(I)** and growth inhibition rates (% ± SE) **(II)** that were achieved using of tested human pathogens controlled by **M1**(CMC-Na:SA (4:1)/0.4% $PdCl_2$), **M2** (CMC-Na:SA (4:1)/0.4% $PdCl_2$/0.15%Cr), **M3** (CMC-Na:SA (4:1)/0.4% $PdCl_2$/0.3%Cr), **M4** (CMC-Na:SA (4:1)/0.4% $PdCl_2$/0.6%Cr), **M5** (CMC-Na:SA (4:1)/0.15%Cr), **M6** (CMC-Na:SA (4:1)/0.3%Cr), **M7** (CMC-Na:SA (4:1)/0.6% Cr); against human pathogens: *Salmonella paratyphi* (***A***), *Escherichia coli* (***B***), *Pseudomonas aeruginosa* (***C***), *Staphylococcus epidermidis* (***D***), *Staphylococcus aureus* (***E***), *Bacillus cereus* (***F***), *Candida krusei* (***G***), *Candida tropicals* (***H***), *and Candida glabrata* (***J***). Asterisks signify a difference that was around 5% significant. Two stars (**) indicate statistically significant differences (P-value < 0.05), whereas one star denotes (*) differences that seem to be statistically significant (P-value = 0.05)

Table 4 Calculated growth inhibition rate (% ± SD) of tested composite hydrogels against human pathogens

Multidrug-resistant human pathogens	Growth inhibition rate (% ± SD)						
	M1	M2	M3	M4**	M5*	M6	M7
Salmonella paratyphi	12.5 ± 2.34c	16.91 ± 1.76c	25 ± 0.25b	37.5 ± 201a	33.08 ± 8.23ab	27.20 ± 5.88ab	30.14 ± 7.05ab
Escherichia coli	10.43 ± 4.78c	32.75 ± 3.62c	40.86 ± 9.56b	72.75 ± 3.62a	69.85 ± 5.07ab	67.53 ± 6.23ab	66.37 ± 6.81ab
Pseudomonas aeruginosa	2.68 ± 9.48c	25.67 ± 2.37c	39.60 ± 8.80b	77.50 ± 6.11a	70.90 ± 4.64ab	68.70 ± 4.15ab	68.48 ± 4.10ab
Staphylococcus epidermidis	0.32 ± 0.67c	16.99 ± 3.46c	68.62 ± 7.45b	81.69 ± 9.34a	37.58 ± 1.69ab	36.92 ± 8.10ab	37.25 ± 4.90ab
Staphylococcus aureus	26.09 ± 6.49c	51.53 ± 5.08c	67.54 ± 3.85b	78.50 ± 8.77a	69.07 ± 8.94ab	66.66 ± 7.66ab	54.82 ± 4.56ab
Bacillus cereus	2.26 ± 0.53c	6.47 ± 2.49c	53.07 ± 4.43b	81.55 ± 3.39a	64.72 ± 4.91ab	62.45 ± 9.54ab	61.81 ± 2.29ab
Candida krusei	3.96 ± 0.47c	10.57 ± 2.68c	50.88 ± 10.57b	65.63 ± 8.76a	58.81 ± 5.72ab	57.70 ± 9.25ab	56.16 ± 7.41ab
Candida tropicals	3.08 ± 0.64c	5.86 ± 4.19c	8.33 ± 3.33b	46.91 ± 3.58a	40.12 ± 3.45ab	39.50 ± 6.17ab	38.58 ± 0.24ab
Candida glabrata	6.77 ± 1.61c	18.27 ± 5.15c	27.3 ± 10.06b	62.42 ± 2.99a	54.00 ± 4.10ab	52.97 ± 7.41ab	50.92 ± 4.02ab

A symbol (*) indicates 5% significant difference. One star (*) implies statistically significant differences (P-value = 0.05), whereas two stars (**) signify significant differences (P-value < 0.05)

Table 5 Biofilm inhibition of tested composite hydrogels against human pathogens

Multidrug-resistant human pathogens	Biofilm inhibition (% ± SD)						
	M1	M2	M3	M4	M5	M6	M7
Salmonella paratyphi	21.51 ± 3.62d	28.34 ± 4.79cd	46.76 ± 12.49ab	53.06 ± 1.94a	52.40 ± 1.57ab	43.58 ± 5.79ab	40.98 ± 5.95cb
Escherichia coli	28.79 ± 7.55d	33.34 ± 6.54cd	44.45 ± 7.02ab	56.70 ± 2.03a	55.15 ± 8.41ab	51.49 ± 2.66ab	45.18 ± 1.01cb
Pseudomonas aeruginosa	22.33 ± 3.80d	33.83 ± 3.74cd	47.34 ± 3.21ab	58.26 ± 1.05a	54.63 ± 9.78ab	50.19 ± 2.29ab	43.94 ± 6.21cb
Staphylococcus epidermidis	25.48 ± 5.75d	28.58 ± 7.98cd	52.49 ± 3.04ab	64.19 ± 1.23a	59.21 ± 9.67ab	51.11 ± 7.45ab	49.16 ± 4.91cb
Staphylococcus aureus	33.80 ± 9.30d	44.12 ± 4.09cd	63.34 ± 1.25ab	76.63 ± 2.43a	73.59 ± 7.24ab	62.94 ± 6.20ab	50.31 ± 1.61cb
Bacillus cereus	37.72 ± 8.93d	42.27 ± 5.31cd	58.56 ± 2.71ab	73.97 ± 6.82a	68.28 ± 6.38ab	63.72 ± 8.12ab	57.57 ± 4.80cb
Candida krusei	43.18 ± 4.66d	53.76 ± 9.46cd	62.88 ± 8.41ab	65.70 ± 3.72a	61.13 ± 1.63a	59.90 ± 2.86ab	50.59 ± 2.4cb
Candida tropicals	21.93 ± 8.81d	32.45 ± 7.05cd	38.94 ± 3.85ab	50.40 ± 6.28a	49.33 ± 1.49a	48.23 ± 9.44ab	45.10 ± 3.78cb
Candida glabrata	23.48 ± 4.63d	34.21 ± 9.83cd	31.45 ± 9.18ab	51.61 ± 3.45a	49.87 ± 1.35ab	47.68 ± 1.11ab	36.31 ± 2.78cb

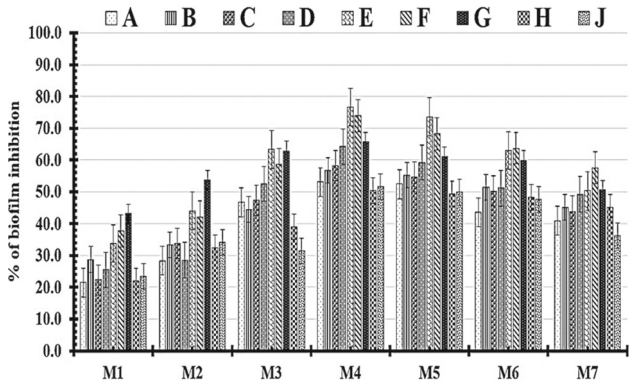

Fig. 12 Calculated biofilm inhibition (%) of tested human pathogens: *Salmonella paratyphi* (**A**), *Escherichia coli* (***B***), *Pseudomonas aeruginosa* (***C***), *Staphylococcus epidermidis* (***D***), *Staphylococcus aureus* (***E***), *Bacillus cereus* (***F***), *Candida krusei* (***G***), *Candida tropicals* (***H***), *and Candida glabrata* (***J***) that controlled by tested formulations **M1**(CMC-Na:SA 4:1 + 0.4% PdCl2), **M2** (CMC-Na:SA 4:1 + 0.4% PdCl2 + 0.15%Cr), **M3** (CMC-Na:SA 4:1 + 0.4% PdCl2 + 0.3%Cr), **M4** (CMC-Na:SA 4:1 + 0.4% PdCl2 + 0.6%Cr), **M5** (CMC-Na:SA 4:1 + 0.15%Cr), **M6** (CMC-Na:SA 4:1 + 0.3%Cr), **M7** (CMC-Na:SA 4:1 + 0.6%Cr)

curcumin might have stronger antibacterial effects than antifungal efficacy, although the mechanism of action remained unclear [59–61].

4 Conclusions

Microporous CMC-Na/SA/$PdCl_2$ composite hydrogel was effectively prepared and optimized by the gelation method. The valuable condition of optimization to fabricate crosslinked CMC-Na/SA hydrogel membrane with a best percentage of gel fraction was CMC-Na:SA (4:1)/0.4% $PdCl_2$. The optimum formula produced a gel fraction of 91% with the swelling ratio of 3040% at 96 h. The present study supplied a promising localized candidate with anticancer activity against propagation of liver cancer, when employing an optimized composite membrane. It is noticed that CMC-Na/SA/$PdCl_2$ hydrogel membrane demonstrated more anticancer activity than curcumin-loaded CMC-Na/SA/$PdCl_2$. The cytotoxic effect on *HePG-2* is more than *MDA-MB231 and CaCo-2*. Also, this current study provided a promising localized antimicrobial activity when applying CMC-Na:SA (4:1)/0.4% $PdCl_2$/0.6% curcumin. It has the maximum biofilm inhibition that was recorded against *Staphylococcus aureus* (77%), followed by *Bacillus cereus* (74%) and *Candida krusei* (66%).

Supplementary Information The online version contains supplementary material available at https://doi.org/10.1007/s13369-024-09233-w.

Acknowledgements This study is supported via funding from Prince Sattam bin Abdulaziz University Project No. (PSAU/2023/R/1445).

Author Contributions Mariam Imam contributed to experimental work and wrote the original manuscript; Samar Salim performed supervision, wrote the original, and revised the manuscript; Shahira El-Moslamy conducted the microbiology part; Nehal El-Deeb conducted the cell culture experiments; A.K. El-Sawaf and A.A. Nassar contributed to materials and part funding for characterization; and Elbadawy Kamoun performed supervision, wrote the original, and revised the final manuscript.

Funding No funding was received for conducting this work.

Data Availability All data are available.

Declarations

Conflict of interests The authors declare that they have no conflict of interest.

Ethical Approval No animal model, human trials nor in vivo experiments were carried out in this research, while all research studies followed the Helsinki World Medical Association's Declaration: Ethical Medical Research Principles Involving Human Subjects.

Consent for Publications Not applicable.

References

1. Kesharwani, P.; Bisht, A.; Alexander, A.; Dave, V.; Sharma, S.: Biomedical applications of hydrogels in drug delivery system: An update. J Drug Deliv Sci Technol **66**(June), 102914 (2021). https://doi.org/10.1016/j.jddst.2021.102914
2. Song, Y.; Xu, L.; Xu, L.; Deng, L.: Radiation cross-linked gelatin/sodium alginate/carboxymethylcellulose sodium hydrogel for the application as debridement glue paste. Polym Bull. **79**(2), 725–742 (2022). https://doi.org/10.1007/s00289-020-03525-5
3. Janarthanan, G.; Noh, I.: Recent trends in metal ion based hydrogel biomaterials for tissue engineering and other biomedical applications. J. Mater. Sci. Technol. **10**(63), 35–53 (2021)
4. Pellá, M.C.G.; Lima-Tenório, M.K.; Tenório-Neto, E.T.; Guilherme, M.R.; Muniz, E.C.; Rubira, A.F.: Chitosan-based hydrogels: from preparation to biomedical applications. Carbohydr Polym. **196**(March), 233–245 (2018). https://doi.org/10.1016/j.carbpol.2018.05.033
5. Hu, W.; Wang, Z.; Xiao, Y.; Zhang, S.; Wang, J.: Advances in crosslinking strategies of biomedical hydrogels. Biomater. Sci. **7**(3), 843–855 (2019)
6. Tang, P.; Wu, J.; Guo, Z.; Liu, W.: MIL-88A-based antifouling superhydrophilic membrane for efficient emulsion separation and dye degradation via photo-fenton process. Surf. Interf. **1**(43), 103572 (2023)
7. Walbrück, K.; Kuellmer, F.; Witzleben, S.; Guenther, K.: Synthesis and characterization of PVP-stabilized palladium nanoparticles by XRD, SAXS, SP-ICP-MS, and SEM. J. Nanomater. **2019**, 1–7 (2019)
8. Lazarević, T.; Rilak, A.; Bugarčić, ŽD.: Platinum, palladium, gold and ruthenium complexes as anticancer agents: current clinical uses, cytotoxicity studies and future perspectives. Eur. J. Med. Chem. **142**, 8–31 (2017)
9. Phan, T.T.V.; Huynh, T.C.; Manivasagan, P.; Mondal, S.; Oh, J.: An up-to-date review on biomedical applications of palladium nanoparticles. Nanomaterials **10**(1), 66 (2020)
10. Baghayeri, M.; Alinezhad, H.; Tarahomi, M.; Fayazi, M.; Ghanei-Motlagh, M.; Maleki, B.: A non-enzymatic hydrogen peroxide

sensor based on dendrimer functionalized magnetic graphene oxide decorated with palladium nanoparticles. Appl. Surf. Sci. **1**(478), 87–93 (2019)
11. Baghayeri, M.; Veisi, H.; Veisi, H.; Maleki, B.; Karimi-Maleh, H.; Beitollahi, H.: Multi-walled carbon nanotubes decorated with palladium nanoparticles as a novel platform for electrocatalytic sensing applications. RSC Adv. **4**(91), 49595–49604 (2014)
12. Ray, S.; Mohan, R.; Singh, J.K.; Samantaray, M.K.; Shaikh, M.M.; Panda, D., et al.: Anticancer and antimicrobial metallopharmaceutical agents based on palladium, gold, and silver N-heterocyclic carbene complexes. J. Am. Chem. Soc. **129**(48), 15042–15053 (2007)
13. Wang, Y.; Zheng, Y.; He, W.; Wang, C.; Sun, Y.; Qiao, K.; Wang, X.; Gao, L.: Preparation of a novel sodium alginate/polyvinyl formal composite with a double crosslinking interpenetrating network for multifunctional biomedical application. Compos. B Eng. **15**(121), 9–22 (2017)
14. He, X.; Zeng, L.; Cheng, X.; Yang, C.; Chen, J.; Chen, H.; Ni, H.; Bai, Y.; Yu, W.; Zhao, K.; Hu, P.: Shape memory composite hydrogel based on sodium alginate dual crosslinked network with carboxymethyl cellulose. Eur. Polymer J. **5**(156), 110592 (2021)
15. Ning, L.; Jia, Y.; Zhao, X.; Tang, R.; Wang, F.; You, C.: Nanocellulose-based drug carriers: functional design, controllable synthesis, and therapeutic applications. Int. J. Biol. Macromol. **1**(222), 1500–1510 (2022)
16. Capanema, N.S.; Mansur, A.A.; Carvalho, I.C.; Carvalho, S.M.; Mansur, H.S.: Bioengineered water-responsive carboxymethyl cellulose/poly (vinyl alcohol) hydrogel hybrids for wound dressing and skin tissue engineering applications. Gels. **9**(2), 166 (2023)
17. Wang, Y.; Xiao, D.; Tang, Y.; Xia, Y.; Zhong, Y.; Zhang, L.; Sui, X.; Wang, B.; Feng, X.; Xu, H.; Mao, Z.: Carboxymethyl cellulose-based injectable hydrogel loaded with a composite of melatonin and γ-cyclodextrin with antioxidant property for diabetic wound repair. Cellulose **30**(3), 1791–1810 (2023)
18. Zennifer, A.; Senthilvelan, P.; Sethuraman, S.; Sundaramurthi, D.: Key advances of carboxymethyl cellulose in tissue engineering & 3D bioprinting applications. Carbohydr. Polym. **256**, 117561 (2021)
19. Dahlan, N.A.; Teow, S.Y.; Lim, Y.Y.; Pushpamalar, J.: Modulating carboxymethylcellulose-based hydrogels with superior mechanical and rheological properties for future biomedical applications. Express Polym Lett **15**(7), 612–625 (2021)
20. Koneru, A.; Dharmalingam, K.; Anandalakshmi, R.: Cellulose based nanocomposite hydrogel films consisting of sodium carboxymethylcellulose–grapefruit seed extract nanoparticles for potential wound healing applications. Int. J. Biol. Macromol. **148**, 833–842 (2020)
21. Hu, Y.; Hu, S.; Zhang, S.; Dong, S.; Hu, J.; Kang, L., et al.: A double-layer hydrogel based on alginate-carboxymethyl cellulose and synthetic polymer as sustained drug delivery system. Sci. Rep. **11**(1), 1–14 (2021). https://doi.org/10.1038/s41598-021-88503-1
22. Ren, H.; Gao, Z.; Wu, D.; Jiang, J.; Sun, Y.; Luo, C.: Efficient Pb(II) removal using sodium alginate-carboxymethyl cellulose gel beads: preparation, characterization, and adsorption mechanism. Carbohydr. Polym. **137**, 402–409 (2016)
23. Zhang, K.; Wang, Y.; Wei, Q.; Li, X.; Guo, Y.; Zhang, S.: Design and fabrication of sodium alginate/carboxymethyl cellulose sodium blend hydrogel for artificial skin. Gels **7**(3), 115 (2021)
24. Lu, K.H.; Lu, P.W.A.; Lu, E.W.H.; Lin, C.W.; Yang, S.F.: Curcumin and its analogs and carriers: potential therapeutic strategies for human osteosarcoma. Int. J. Biol. Sci. **19**(4), 1241–1265 (2023)
25. Wang, Y.; Xu, S.; Han, C.; Wang, L.; Zheng, Q.; Wang, S., et al.: Curcumin inhibits Singapore grouper iridovirus infection through multiple antiviral mechanisms. Aquaculture. **562**(September), 738870 (2022). https://doi.org/10.1016/j.aquaculture.2022.738870
26. Hajifathali, S.; Lesan, S.; Lotfali, E.; Salimi-Sabour, E.; Khatibi, M.: Investigation of the antifungal effects of curcumin against nystatin-resistant Candida albicans. Dental Res. J. **20**(1), 50 (2023)
27. Wang, M.; Yi, N.; Fang, K.; Zhao, Z.; Xie, R.; Chen, W.: Deep colorful antibacterial wool fabrics by high-efficiency pad dyeing with insoluble curcumin. Chem. Eng. J. **452**, 139121 (2022)
28. Ilyas, U.; Katare, D.P.; Aeri, V.; Naseef, P.P.: A review on hepatoprotective and immunomodulatory herbal plants. Pharmacogn. Rev. **10**(19), 66–70 (2016)
29. Chopra, H.; Mohanta, Y.K.; Rauta, P.R.; Ahmed, R.; Mahanta, S.; Mishra, P.K.; Panda, P.; Rabaan, A.A.; Alshehri, A.A.; Othman, B.; Alshahrani, M.A.: An insight into advances in developing nanotechnology based therapeutics, drug delivery, diagnostics and vaccines: multidimensional applications in tuberculosis disease management. Pharmaceuticals **16**(4), 581 (2023)
30. Abadi, A.J.; Mirzaei, S.; Mahabady, M.K.; Hashemi, F.; Zabolian, A.; Hashemi, F., et al.: Curcumin and its derivatives in cancer therapy: potentiating antitumor activity of cisplatin and reducing side effects. Phyther Res. **36**(1), 189–213 (2022)
31. Hussein, Y.; Loutfy, S.A.; Kamoun, E.A.; EL-Moslamy, S.H.; Radwan, E.M.; Elbehairi, S.E.I.: Enhanced anti-cancer activity by localized delivery of curcumin form PVA/CNCs hydrogel membranes: preparation and in vitro bioevaluation. Int. J. Biol. Macromol. **170**, 107–122 (2021)
32. Agarwal, T.; Narayana, S.N.G.H.; Pal, K.; Pramanik, K.; Giri, S.; Banerjee, I.: Calcium alginate-carboxymethyl cellulose beads for colon-targeted drug delivery. Int. J. Biol. Macromol. **75**, 409–417 (2015)
33. Tang, X.; Wang, X.; Sun, Y.; Zhao, L.; Li, D.; Zhang, J., et al.: Magnesium oxide-assisted dual-cross-linking bio-multifunctional hydrogels for wound repair during full-thickness skin injuries. Adv. Funct. Mater. **31**(43), 1–11 (2021)
34. Ibrahim, S.M.; El Salmawi, K.M.: Preparation and properties of carboxymethyl cellulose (CMC)/sodium alginate (SA) blends induced by gamma irradiation. J. Polym. Environ. **21**(2), 520–527 (2013)
35. Benamer, S.; Mahlous, M.; Boukrif, A.; Mansouri, B.; Youcef, S.L.: Synthesis and characterisation of hydrogels based on poly(vinyl pyrrolidone). Nucl. Instr. Meth. Phys. Res. Sect. B Beam Interact Mater. Atoms. **248**(2), 284–290 (2006)
36. Gradilla-Orozco, J.L.; Hernández-Jiménez, J.Á.; Robles-Vásquez, O.; Cortes-Ortega, J.A.; Renteria-Urquiza, M.; Lomelí-Ramírez, M.G., et al.: Physicomechanical and morphological characterization of multi-structured potassium-acrylate-based hydrogels. Gels **8**(10), 1–14 (2022)
37. Salim, S.A.; Badawi, N.M.; EL-Moslamy, S.H.; Kamoun, E.A.; Daihom, B.A.: Novel long-acting brimonidine tartrate loaded-PCL/PVP nanofibers for versatile biomedical applications: fabrication, characterization and antimicrobial evaluation. RSC Adv. **13**(22), 14943–14957 (2023)
38. Chauhan, S.; Bansal, M.; Khan, G.; Yadav, S.K.; Singh, A.K.; Prakash, P., et al.: Development, optimization and evaluation of curcumin loaded biodegradable crosslinked gelatin film for the effective treatment of periodontitis. Drug development and industrial pharmacy, Vol. 44, p. 1212–1221. Taylor and Francis, Routledge (2018)
39. Hayat, S.; Ashraf, A.; Zubair, M.; Aslam, B.; Siddique, M.H.; Khurshid, M., et al.: Biofabrication of ZnO nanoparticles using Acacia arabica leaf extract and their antibiofilm and antioxidant potential against foodborne pathogens. PLoS One. **17**(1 January), 1–18 (2022)
40. Balows, A.: Manual of clinical microbiology 8th edition: P. R. Murray, E. J. Baron, J. H. Jorgenson, M. A. Pfaller, and R. H. Yolken, eds., ASM Press, 2003, 2113 pages, 2 vol, 2003 + subject & author indices, ISBN: 1–555810255–4, US$ 189.95. Diagn Microbiol Infect Dis. **47**(4), 625 (2003)

41. Feizi, H.; Agheli, N.; Sahabi, H.: Titanium dioxide nanoparticles alleviate cadmium toxicity in lentil (Lens culinaris Medic) seeds. Acta Agric Slov. **116**(1), 59–68 (2020)
42. Hawkins, A.N.; Licea, S.J.; Sleeper, S.A.; Swearingen, M.C.: Calcium sulfate beads made with antibacterial essential oil-water emulsions exhibit growth inhibition against Staphylococcus aureus in agar pour plates. PLoS One **17**(7 July), 4–13 (2022)
43. Cruz, C.D.; Shah, S.; Tammela, P.: Defining conditions for biofilm inhibition and eradication assays for Gram-positive clinical reference strains. BMC Microbiol **18**(1), 1–9 (2018)
44. Dai, H.; Ou, S.; Huang, Y.; Liu, Z.; Huang, H.: Enhanced swelling and multiple-responsive properties of gelatin/sodium alginate hydrogels by the addition of carboxymethyl cellulose isolated from pineapple peel. Cellulose **25**(1), 593–606 (2018)
45. Ibrahim, S.M.; Abou El Fadl, F.I.; EL-Naggar, A.A.: Preparation and characterization of crosslinked alginate-CMC beads for controlled release of nitrate salt. J. Radioanal. Nucl. Chem. **299**(3), 1531–1537 (2014)
46. Hussein, Y.; Loutfy, S.A.; Kamoun, E.A.; EL-Moslamy, S.H.; Radwan, E.M.; Elbehairi, S.E.I.: Enhanced anti-cancer activity by localized delivery of curcumin form PVA/CNCs hydrogel membranes: preparation and in vitro bioevaluation. Int. J. Biol. Macromol. **170**(December), 107–122 (2021)
47. Rajasekharreddy, P.; Rani, P.U.: Biosynthesis and Characterization of Pd and Pt Nanoparticles Using Piper betle L Plant in a Photoreduction Method. J Clust Sci. **25**(5), 1377–1388 (2014)
48. Tuan Mohamood, N.F.A.Z.; Abdul Halim, A.H.; Zainuddin, N.: Carboxymethyl cellulose hydrogel from biomass waste of oil palm empty fruit bunch using calcium chloride as crosslinking agent. Polymers (Basel). **13**(23), 4056 (2021)
49. Badita, C.R.; Aranghel, D.; Burducea, C.; Mereuta, P.: Characterization of sodium alginate based films. Rom. J. Phys. **65**(1–2), 1–8 (2020)
50. Abd El-Hady, M.M.; El-Sayed Saeed, S.: Antibacterial properties and pH sensitive swelling of insitu formed silver-curcumin nanocomposite based chitosan hydrogel. Polymers. **12**, 1–14 (2020)
51. Yang, Y.; Yu, X.; Zhu, Y.; Zeng, Y.; Fang, C.; Liu, Y.: Preparation and application of a colorimetric film based on sodium alginate/sodium carboxymethyl cellulose incorporated with rose anthocyanins. Food Chem. **393**(May), 133342 (2022)
52. El-Bana, A.A.; Barakat, N.M.; Abdelghany, A.M.; Meikhail, M.S.: Effect of surfactants addition on physical, structure and antimicrobial activity of (Na-CMC/Na–Alg) biofilms. Polym. Bull. **80**(3), 2883–2909 (2022)
53. Bajpai, S.K.; Chand, N.; Ahuja, S.: Investigation of curcumin release from chitosan/cellulose micro crystals (CMC) antimicrobial films. Int. J. Biol. Macromol. **79**, 440–448 (2015)
54. Patel, N.; Lalwani, D.; Gollmer, S.; Injeti, E.; Sari, Y.; Nesamony, J.: Development and evaluation of a calcium alginate based oral ceftriaxone sodium formulation. Prog. Biomater. **5**(2), 117–133 (2016)
55. Kang, H.; Gao, J.; Xie, M.; Sun, Y.; Wu, F.; Gao, C., et al.: Carboxymethyl cellulose gel membrane loaded with nanoparticle photocatalysts for hydrogen production. Int. J. Hydr. Energy **44**(26), 13011–13021 (2019)
56. Czarnomysy, R.; Radomska, D.; Szewczyk, O.K.; Roszczenko, P.; Bielawski, K.: Platinum and palladium complexes as promising sources for antitumor treatments. Int. J. Mol. Sci. **22**(15), 8271 (2021)
57. Ashraf, H.; Salim, S.A.; EL-Moslamy, S.H.; Loutfy, S.A.; Kamoun, E.A.: An Injectable in situ forming collagen/alginate/$CaSO_4$ composite hydrogel for tissue engineering applications: optimization characterization and in vitro assessments. Arab. J. Sci. Eng. (2024). https://doi.org/10.1007/s13369-024-08922-w
58. Rodrigues, M.A.; Fernandes, J.N.; Ruggiero, R.; Guerra, W.: Palladium complex containing curcumin as ligand: thermal and spectral characterization. Am. J. Chem. **2**(3), 157–159 (2012)
59. Zianna, A.; Geromichalos, G.; Fiotaki, A.M.; Hatzidimitriou, A.G.; Kalogiannis, S.; Psomas, G.: Palladium(II) complexes of substituted salicylaldehydes: synthesis, characterization and investigation of their biological profile. Pharmaceuticals **15**(7), 886 (2022)
60. Saravanan, A.; Kumar, P.S.; Karishma, S.; Vo, D.V.N.; Jeevanantham, S.; Yaashikaa, P.R., et al.: A review on biosynthesis of metal nanoparticles and its environmental applications. Chemosphere **264**, 128580 (2021)
61. Alloosh, M.T.; Khaddam, W.I.; Almuhammady, A.K.: Biosynthesis of metal nanoparticles using microorganisms and its medicinal applications. Nov. Res. Microbiol. J. **5**(1), 1077–1090 (2021)